ATMOSPHERIC RESEARCH

RECHERCHE ATMOSPHÉRIQUE

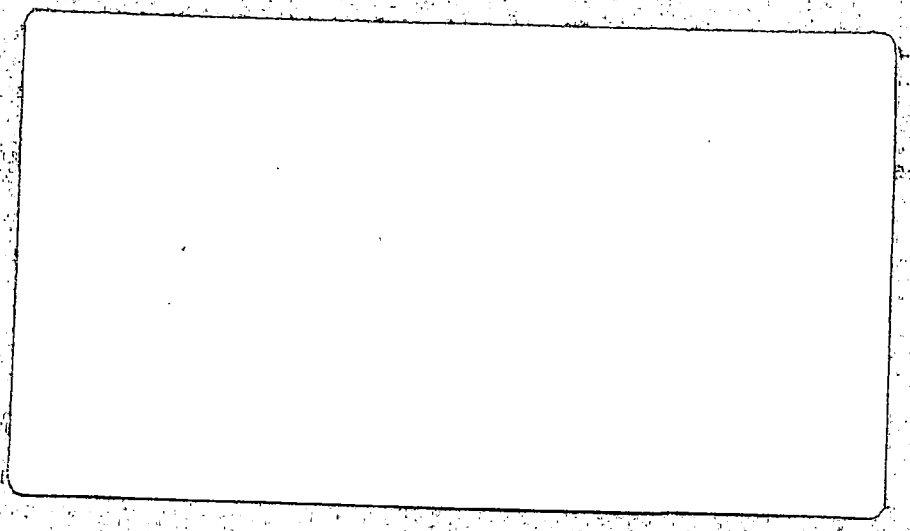

ATMOSPHERIC ENVIRONMENT

ENVIRONNEMENT ATMOSPHÉRIQUE

Report - ARQL - 76/4 December 1976

Advances in Three-Dimensional Mesoscale Modelling in the Boundary Layer Research Division, 1976

John L. Walmsley
and
John D. Reid

This is one of a series of internal reports prepared by the Atmospheric Research Directorate.

The views expressed in this document reflect the opinion of the individual contributors and do not necessarily represent the official position of the Atmospheric Environment Service.

It should not be referenced or quoted without the written permission of the authors.

Air Quality and Inter-Environmental Research Branch
Atmospheric Environment Service
4905 Dufferin Street
Downsview, Ontario
M3H 5T4

Table of Contents

Abstract

This report documents progress to December 1976 in three-dimensional and time-dependent mesoscale numerical modelling for air quality studies. Current operational models used in such studies and mesoscale air flow models are reviewed. One such mesoscale model, the University of Virginia (Pielke) model, is considered in particular.

Development of the physical equations, transformation of the vertical coordinate and numerical techniques employed are treated in detail and deficiencies indicated. Application of the model on the AES CYBER 76 computer to simple cases is discussed to highlight model capabilities and deficiencies. The application to air quality studies is illustrated. Finally this work is summarized and future plans outlined.

Résumé

Ce rapport indique le progrès jusqu'à décembre 1976 sur l'élaboration, dans le but d'études sur la qualité de l'air, de modèles tridimensionels à function du temps. On passe en revue des modèles d'exploitation utilisés couramment pour telles études aussi bien que des modèles d'écoulement de l'air à moyenne échelle. On considère un tel modèle en particulier, celui de l'Université de la Virginie (développé par Pielke).

Le développement des équations physiques, la transformation de la coordonnée verticale et les techniques numériques employées sont traités en détail. Les insuffisances du modèle sont indiquées. On discute l'application du modèle, utilisant l'ordinateur CYBER 76 du SEA, à quelques expériences non-compliqueés afin de souligner les capacités et les insuffisances du modèle. On explique l'application aux études sur la qualité de l'air. Enfin, on résume le progrès sommairement et on indique des plans de l'avenir.

Acknowledgments

For a number of years now our Director, Dr. M. Kwizak has supported and encouraged numerical modelling on urban and regional scales. The modelling research and development which are the subjects of the present report have thrived in such an environment.

It is a pleasure to acknowledge the interest and encouragement of Dr. G.A. McBean at all stages of this work. We have also benefitted from several useful discussions with Dr. W. Cotton of Colorado State University.

Dr. R.A. Pielke of the University of Virginia kindly provided a computer listing of his model, gave permission to obtain a copy of the model on computer cards from NCAR and sent us a draft of a recent paper.

Mr. G. Blair of Atmospheric Processes Research Branch assisted us in adapting the computer version of the model to the "automatic submission" mode which has saved us many days of "turn-around" time.

Finally, we are grateful to Mr. B. Taylor who drafted the diagrams and to Mrs. K. Ford who did an excellent job of transcribing two different hand-writings into neat, legible typescript.

CHAPTER I

INTRODUCTION

This report documents progress within the Boundary Layer Research Division to December 1976 in three-dimensional, time-dependent mesoscale numerical modelling and plans for future activity. The effort is motivated by a requirement to improve Air Quality and Inter-Environmental Research Branch's capability to model actual situations of air pollution transport, dispersion, and depletion. Modelling activity within the Division received considerable impetus in May 1976 with the addition of five scientists. Two of these scientists, the current authors, embarked upon a project to evaluate the University of Virginia's mesoscale (Pielke) model for the Branch's needs.

Chapter II surveys current operational models used in air quality studies. Research three-dimensional mesoscale models, either developed or under development, are discussed as they apply to air quality problems.

Chapter III details the development of the physical equations. The transformations to the vertical coordinate and numerical techniques employed in the model are then discussed. Finally, the model deficiencies are indicated.

Chapter IV details the extensive testing of the model on a variety of simple cases which give valuable insight into the sensitivity of the results, particularly to initialization and boundary conditions.

Chapter V shows some results from the model airflow predictions applied to the calculation of air pollution trajectories for a simple lake or sea breeze situation. The importance to inland air quality of pollution sources along the shore for this idealized case is discussed.

Finally, in Chapter VI, the work reported here is summarized and its importance for air quality applications emphasized. General and specific conclusions are identified and plans for future model development indicated.

CHAPTER II

SURVEY OF PRESENT MODELS

2.1. Current Air Quality Models

The last decade has seen widespread concern regarding Man's impact on the environment. Numerous indicators bear witness to severe inadvertent environmental effects. This concern is now embodied in legislation in several jurisdictions requiring assessment of environmental impacts of proposed projects, and restricting emissions of air pollutants. Soundly based assessments can only be achieved, however, through understanding of physical processes affecting air quality. Increasing sophistication of models has led to their general acceptance as valid techniques in air quality assessment.

While this report is primarily concerned with detailing progress in mesoscale meteorological modelling, this effort, undertaken in support of air quality objectives, is viewed in the perspective of current air quality modelling practices.

2.1.1. Statistical Models

The initial attempts at air quality assessment were based on statistical techniques. These are developed by correlation between measured air quality data, emission inventories and meteorological data. Since no cause and effect relationship is invoked, the range of validity of the resulting predictive procedure is limited. No ability to assess the impact of additional individual pollution sources results.

2.1.2. Box Models

A second type of model, more physically based, is that generally described as a box model. The basic assumption is that a box of specified volume is defined inside which any pollutant is uniformly mixed.

2.1.2.1. Eulerian Box Models

One way in which the box can be defined is by a terrain constraint on mixing (such as in a mountain canyon, or the Decarie Expressway in Montreal). The top of the box is given by some assumed inversion restricting vertical transport of pollutant. Concentration of pollutant is determined from continuity, dividing the volume of the box into the total mass of pollutant in it. Concentration changes can be related to emission rates, chemical species transformation rates and physical depletion rates. In some cases a crude ventilation effect can be incorporated. The assumption of uniform mixing is quite restrictive. Measurements suggest that this is rarely the case. Further, it is a rather exceptional case that permits definition of a topographically constrained box in any meaningful sense.

2.1.2.2 Lagrangian Box Models

Another type of box model is the "Lagrangian Box", sometimes called "Trajectory" Model. A box moving with the wind in the lower levels is considered. Winds may be derived from observation or a meteorological model. Continuity is again invoked to permit calculation of concentrations. Some additional assumptions are necessary. The pollution emissions are expressed per unit area, thus removing dependence on the horizontal dimensions of the box. Net changes in pollutant in the box due to eddy fluxes through its sides are assumed to be negligible. This demands that the areal distribution of pollution sources be rather uniform. A careful evaluation of this type model by Liu and Seinfeld (1974) showed that the largest source of error in this model resulted from the assumption that the box moved with a wind representative of the entire mixed layer. Vertical windshear was found to be important. It is noteworthy that analogous inaccuracies can be expected to arise for airflow prediction in dynamic equations formulated with a mixed layer assumption.

A particularly innovative application of this trajectory model has been made by Summers (1964) who considered the effect of city thermal sources in increasing the mixed depth over the city as air passes over it.

2.1.3. The Gaussian Plume Model

Currently the most used models are variants of the Gaussian Plume Model, so called because the cross-wind and vertical distributions of pollutant concentration from a continuous point source are specified as Gaussian. A Gaussian concentration profile can be obtained theoretically from the equation of continuity for conditions of uniform wind and turbulence fields, without sink processes. Although these conditions are not met in the atmospheric boundary layer, a Gaussian plume is nevertheless found to give a reasonable representation of pollution concentrations averaged over several minutes for uniform terrain and steady airflow conditions.

The most commonly employed Gaussian formulation for ground level receptors is

$$\bar{\chi} = \frac{Q}{\pi \sigma_y \sigma_z \bar{U}} \exp\left[-\left(\frac{y^2}{2\sigma_y^2} + \frac{h^2}{2\sigma_z^2}\right)\right]$$

where

- $\bar{\chi}$ is the pollutant concentration at (x, y)
- Q is the pollutant emission rate
- $\bar{U}$ is the mean wind speed
- h is the effective source height (including plume rise) above the ground
- x is downwind distance of the receptor from the source
- y is cross-wind distance of the receptor from the wind vector through the source
- σ_y, σ_z are the cross-wind and vertical standard deviations of the concentration distribution, functions of x and averaging time for any particular meteorological condition.

This equation is based on the assumption that any pollutant impacting the surface is reflected by it. Standard deviations required have been obtained in several investigations, the most commonly employed being a graphical presentation based on six classes of meteorological categories, Pasquill's "stability" classes A through F.

The Gaussian plume formulation is sufficiently widely employed that it has been formalized in a number of computer programs, for example, the Air Quality Display Model (AQDM), and Climatic Dispersion Model (CDM), both from the U.S. Environmental Protection Agency. However, this widespread use certainly constitutes abuse. The ideal nature of the topography over which the standard deviations employed were obtained is not often matched by the sites at which they are employed.

2.2. Mesoscale Meteorological Modelling for Air Quality

The deficiencies of currently employed air quality models have been noted. What kind of model is appropriate for air quality work? It is not too difficult to specify a model that would do the job - but this would be impractical in today's computer environments. This ideal model would give information on pollutant concentrations at all spatial and temporal scales. Fortunately, there is little requirement for fine spatial and temporal resolution air quality predictions. However, while the air quality resolution requirement can be relaxed, the effects of the smaller scale winds on pollutant dispersal must be maintained. Naturally, the smaller the scale cut-off of the resolved winds, the better will be the prediction.

A second requirement for an air quality model is that it gives especial attention to the flow and forcing occurring within the planetary boundary layer as the vast majority of air quality problems arise for pollutants which never leave these low levels. This fact gives such modelling special problems, not encountered in, say, weather forecast, general circulation, or cloud physics models, where drag coefficient formulations of boundary layer processes suffice. On the other hand, it also implies that the treatment of regions away from the boundary layer can be relaxed to the extent that errors resulting in the boundary layer are acceptable.

Probably the most widely adopted assumption is that the presence of the pollutant does not affect the airflow. A few exploratory investigations on modification to flow resulting from pollutant interacting radiatively have been undertaken, and this effect may be important under some conditions. However, the assumption of a passive pollutant simplifies the calculations for three-dimensional and time-dependent cases considerably. In particular, because computations of airflow and turbulence can be performed independently of the dispersion computations, the full resources of the computer can be devoted to the meteorological computations. This permits greater field resolution and/or faster computer execution as well as dispersion investigations for a variety of source configurations without repeating the flow solution calculations.

The Navier-Stokes equations predict the evolution of a fluid dynamical system, such as the earth's atmosphere. Unfortunately, because atmospheric phenomena occur on a wide range of scales, particularly small scales, it is impractical to apply these equations without modification. The usual approach is to specify the dependent variables as sums of an average and deviation component. It is then possible to formulate the Reynolds equations for the evolution of averaged quantities which contain only averaged quantities.

Satisfactory handling of the Reynolds stress terms in the Reynolds equations is the outstanding problem of numerical modelling of the atmosphere today. The difficulty which arises is that, although predictive equations for the stresses can be derived, they do not form a closed set. Instead triple correlation terms arise which have to be parameterized. To date such second-order-closure methods have not been applied to mesoscale three-dimensional and time-dependent situations, and so these methods will not be discussed further here. Interested readers are referred to papers by Busch (1973), Deardorff (1973), Lumley and Khajeh-Nouri (1974), Wyngaard and Coté (1974), and Yamada and Mellor (1975).

A more traditional approach to closure is to adopt the first order eddy viscosity (K) scheme. The motivation for this closure rests on analogy between viscous dissipation of air motion to heat, which can be successfully expressed as a gradient transport process, and the cascade of kinetic energy to smaller and smaller scales. Although this is a simple closure it has performed with considerable success in numerous models, each with seemingly a different formulation for eddy viscosity.

Smagorinsky (1963) suggested a form

$$K = .02\ \Delta^2\ D$$

where Δ is the grid spacing and D the magnitude of the mean flow deformation tensor. This form is most appropriate when Δ is within the inertial subrange, less than $\sim$ 100 m. This resolution is too fine to permit strict application to mesoscale models on available computers. Nevertheless, lacking any better formulation similar types of expressions are commonly employed for horizontal eddy viscosity, see for example Pielke (1973), Estoque et al. (1976). This type of parameterization appears to suffice for horizontal grid spacings typically employed in mesoscale models 0 (10 km) with solutions fairly insensitive to K_H which is small in magnitude.

Vertical eddy viscosity is better represented in the boundary layer of mesoscale models by a specified eddy viscosity profile. This is because typical averaged vertical velocities are small (compared to horizontal velocities) so that in the vertical a more significant part of the transport occurs on the unresolved eddy scales. Typically a specified vertical profile for K_z is employed using well-documented results in the surface layer [see for example the review by McBean (1976)] and curve fitting to small values at the top of the boundary layer. A cubic polynomial expression formulated by O'Brien (1970) has recently gained increasing acceptance.

It is a matter of everyday experience that the nature of the lower surface has a considerable influence on the airflow above it. Specifically, variations in terrain height govern a variety of phenomena, valleys channel the wind direction and surface breezes blow up and down terrain slopes. It is clearly important to handle terrain variation carefully in mesoscale models. Experience using geometric height as vertical coordinate has shown that substantial errors in different approximations to derivatives and boundary conditions can arise near the surface for non-uniform terrain. More recent models employ a transformed vertical coordinate system, for example, the Phillips' (1957) sigma system which, by incorporating the effects of topography into the transformed equations permits improved representation of boundary-layer terrain effects.

Observations of mesoscale systems and numerical modelling comparisons between hydrostatic and non-hydrostatic simulations of such systems [Klemp and Lilly (1975), Pielke (1972)] indicate that the hydrostatic assumption can often be usefully invoked. A recent scale analysis by Taylor (1976) confirms that for "gentle" topography the boundary-layer flow can indeed be treated hydrostatically. For models with grid lengths of several kilometers which resolve only mesoscale and larger systems it is fully consistent to modify the governing equations to include a hydrostatic constraint.

One simplification that has been found useful in the past depends on the ability to vertically integrate the governing equations in the planetary boundary layer. Lavoie (1972) considers this technique, applying it to situations where the boundary layer was well mixed, strong surface heating and prevailing airflow conditions. Keyser and Anthes (1976) argue that airflow predictions useful for air quality studies can be made using a vertically integrated model for a wider range of atmospheric situations.

It is clear that for unstable stratification the wind shear in the outer boundary layer is weak, making the vertical integration technique most meaningful here. But it is worth noting that, according to Pielke (1972) it is for just these unstable conditions that the hydrostatic assumption is most inappropriate. As stability increases boundary layer wind shears become greater.

For neutral situations occurring under strong prevailing flow conditions, shears can be important. Air quality predictions can, as noted before, be substantially in error if shear is not properly accounted for. Because the terms appearing in the conservation of species equation also have counterparts in the momentum equation, analogous errors in airflow can be expected to occur for the vertically integrated equation predictions.

Computer limitations have prohibited the development of three-dimensional simulations until the last few years. The early efforts of Thyer (1967) to model valley winds with a vorticity model and Hino (1968) to model dispersion in complex terrain are noteworthy. In the USSR, Shershkov (1972) has developed a comprehensive dry model.

Development of three-dimensional models, including cloud microphysics, is actively being pursued by Nickerson at NOAA in Boulder, Colorado, by Anthes at Pennsylvannia State University, by Deaven at NCAR, and for summer-time situations by Cotton at Colorado State University. Perhaps the best known and developed model for mesoscale simulations is that of Mahrer and Pielke (1976). In the remainder of this report we document this model, show some examples of calculations and suggest improvements.

CHAPTER III

THE PIELKE MODEL

3.1. Governing Equations

The model equations appear in various papers written during the period of development by Pielke. The earliest references describe the three-dimensional sea breeze model with the variables expressed as deviations from the synoptic scale state (Pielke, 1973, 1974a). The equations for both two- and three-dimensional versions were presented in Pielke (1974b). Subsequently, significant changes were made in formulating the model equations. The dependent variables became the total quantities (perturbation plus large-scale value) rather than simply the perturbation. In addition, a prognostic equation for the boundary layer height (attributed to Deardorff, 1974) was added. These changes, along with the new two-dimensional model equations, were given in Pielke and Mahrer (1975). Later stages in model development included the incorporation of topography (with transformation to a terrain-following coordinate system) in the two-dimensional model (Mahrer and Pielke, 1975) and in the three-dimensional version (Mahrer and Pielke, 1976).

A certain amount of searching through the above-mentioned papers is necessary simply to be able to write down the latest version of the governing equations in their most general form. Further effort is required to examine the inherent assumptions by tracing the development of the equations from more fundamental versions. It was decided, therefore, to consolidate the information from Pielke's papers and show the development of the governing equations in this report. The equations are presented in tabular form beginning with the most fundamental version (Table 3.1) and including necessary auxiliary definitions, relations and constants (Table 3.2). Subsequent tables concentrate on the governing equations at various stages of development, incorporating simplifying assumptions and approximations.

Tensor notation is used to express the equations using a minimum of effort. Unrepeated subscripts indicate free variables; the subscript is understood to be either 1, 2 or 3 and the corresponding variable is any one of three vector components or nine second-order tensor components, etc. For example:

$$x_i \equiv (x_1, x_2, x_3) \equiv (x, y, z)$$

$$u_i \equiv (u_1, u_2, u_3) \equiv (u, v, w)$$

$$u_i u_j \equiv (u^2, uv, uw, vu, v^2, vw, wu, vw, w^2).$$

Repeated subscripts imply the Einstein summation convention is in effect (unless otherwise indicated); the equivalent form in vector notation is the dot-product. Thus:

$$u_i u_i = u^2 + v^2 + w^2$$

$$u_j \frac{\partial}{\partial x_j} = u \frac{\partial}{\partial x} + v \frac{\partial}{\partial y} + w \frac{\partial}{\partial z}$$

Two important (and useful) tensors are δ_{ij} and ε_{ijk} (Kronecker's Delta and the Alternating unit tensor, respectively).

They are defined as follows:

$$\delta_{ij} = \begin{cases} 0 & , \quad i \neq j \\ 1 & , \quad i = j \end{cases} \tag{3.1.1}$$

$$\varepsilon_{ijk} = \begin{cases} 0 & , \quad i = j \text{ or } i = k \text{ or } j = k \\ +1 & , \quad (i, j, k) = (1, 2, 3) \text{ or } (2, 3, 1) \text{ or } (3, 1, 2) \\ -1 & , \quad (i, j, k) = (1, 3, 2) \text{ or } (,3\ 2, 1) \text{ or } (2, 1, 3). \end{cases} \tag{3.1.2}$$

Thus

$$g\,\delta_{3i} = \begin{cases} 0 & , \quad i = 1, 2 \\ g & , \quad i = 3 \end{cases} \tag{3.1.3.}$$

$$\varepsilon_{1jk} f_j u_k = f_2 u_3 - f_3 u_2$$

$$\varepsilon_{2jk} f_j u_k = f_3 u_1 - f_1 u_3 \qquad (3.1.4)$$

It can be seen that the alternating unit tensor is equivalent to the cross-product of vector notation.

Table 3.1 shows the Navier-Stokes equations (the three component equations expressed as one equation in tensor form), thermodynamic equation, moisture conservation equation and mass conservation equation (or continuity equation). Similar notations are given in Monin and Yaglom (1971), Haltiner (1971) and Busch (1973). In Table 3.2. appear the definitions of the Coriolis vector, f_j; potential temperature, θ; scaled pressure, π; Equation of State; an equation for the total time derivative of q_s (Haltiner, 1971); a relation between saturation specific humidity and saturation vapour pressure; Clausius-Clapeyron Equation and definitions of latent heat of vaporization and the condensation "switch" (Haltiner, 1971), respectively.

The Navier-Stokes equations consist of terms representing advection/convection, acceleration due to the pressure gradient, acceleration due to gravity, molecular viscous diffusion and Coriolis effects, respectively. The thermodynamic and moisture conservation equations incorporate advection/convection, molecular conductivity/diffusivity, radiation flux divergence (in the thermodynamic equation only) and condensation/latent heat release, respectively. The remaining partial differential equation is the "quasi-Boussinesq" form of the continuity equation.

As a preliminary simplification of these equations, molecular viscous/diffusion effects are assumed negligible in comparison with their eddy diffusive counterparts which will appear in Table 3.5. The radiative flux divergence is not considered in the model at present. Neglect of this physical effect may be questioned in many circumstances (Busch, 1973). Condensation effects are also ignored. As may be seen from the definition of ∇, the condensation terms are only important when the air becomes saturated in a region of upward vertical motion. Their calculation, however, is fairly straightforward; hence there seems to be no reason why they cannot be included in the future. The thermodynamic and moisture equations would thus become coupled and supersaturation would be avoided.

Table 3.1 - Fundamental Governing Equations

$$\frac{\partial u_i}{\partial t} = - u_j \frac{\partial u_i}{\partial x_j} - \frac{1}{\rho} \frac{\partial p}{\partial x_i} - g \delta_{3i} + \nu \frac{\partial^2 u_i}{\partial x_j \partial x_j} - \varepsilon_{ijk} f_j u_k$$

$$\frac{\partial \theta}{\partial t} = - u_j \frac{\partial \theta}{\partial x_j} + \chi_T \frac{\partial^2 \theta}{\partial x_j \partial x_j} - \frac{1}{\rho C_p} \frac{\partial R_j}{\partial x_j} - \nabla \frac{L_v \theta}{C_p T} \left[\frac{dq_s}{dt} \right]$$

$$\frac{\partial q}{\partial t} = - u_j \frac{\partial q}{\partial x_j} + \chi_q \frac{\partial^2 q}{\partial x_j \partial x_j} + \Delta \left[\frac{dq_s}{dt} \right]$$

$$\frac{\partial u_j}{\partial x_j} = 0$$

Table 3.2. - Auxiliary Definitions, Relations and Constants

$$f_j = 2\Omega \{\cos\phi \sin\alpha, \cos\phi \cos\alpha, \sin\phi\}$$

$$\theta = T \left(p_o/p\right)^K$$

$$\pi = C_p \left(p/p_o\right)^K$$

$$K = R/C_p$$

$$\rho = p/RT$$

$$\frac{dq_s}{dt} = \frac{q_s T}{p}\left(\frac{L_v R - C_p R_v T}{C_p R_v T^2 + q_s L_v^2}\right)\omega$$

$$\omega = \frac{dp}{dt}$$

$$q_s = \frac{\varepsilon e_s}{p - (1-\varepsilon) e_s}$$

$$l_s = l_{s_o} \exp\left\{\frac{L_v}{R_v}\left(\frac{1}{T_o} - \frac{1}{T}\right)\right\}$$

$$L_v = L_{v_o} - l_v \left(T - T_o\right)$$

$$\nabla = \begin{cases} 0 & , \quad q < q_s \text{ or } \omega \geq 0 \\ 1 & , \quad q \geq q_s \text{ and } \omega < 0 \end{cases}$$

$$\alpha = 0$$

$$p_o = 100 \text{ k Pa}$$

$$C_p = 1004.64 \text{ J/(kg.K)}$$

$$R = 287.04 \text{ J/(kg.K)}$$

$$\varepsilon = 0.62197$$

$$e_{s_o} = 0.61078 \text{ k Pa}$$

$$T_o = 273.15 \text{ K}$$

$$L_{v_o} = 2.5008 \times 10^6 \text{ J/kg}$$

$$l_v = 2.37 \times 10^3 \text{ J/(kg.K)}$$

$$R_v = 461.50 \text{ J/(kg.K)}$$

In order to follow the development of the pressure gradient term from Table 3.1 to Table 3.3, it is necessary to make certain assumptions regarding variations in the density and temperature fields. Busch (1973) considers deviations of these quantities from a reference state which is hydrostatic, dry adiabatic and horizontally homogeneous. The same assumptions, however, may be made about deviations from some locally defined mean state. Thus, it is assumed that:

$$\begin{aligned} \rho &= \bar{\rho} + \rho' \quad , \quad |\rho'/\bar{\rho}| << 1 \\ T &= \bar{T} + T' \quad , \quad |T'/\bar{T}| << 1 \\ \theta &= \bar{\theta} + \theta' \quad , \quad |\theta'/\bar{\theta}| << 1 \end{aligned} \tag{3.1.5}$$

Hence from the Equation of State,

$$\rho = p/RT \quad ,$$

it is possible to derive

$$(\bar{\rho} + \rho') = \frac{p}{R(\bar{T} + T')}$$

$$\bar{\rho}\,(1 + \rho'/\bar{\rho}) = \frac{p}{R\bar{T}\,(1 + T'/\bar{T})}$$

$$\bar{\rho} \approx \frac{p}{R\bar{T}} \tag{3.1.6}$$

(This equation is equivalent to the form, $\rho'/\bar{\rho} = -T'/\bar{T}$, given by Busch). From the definition of potential temperature,

$$\theta = T\,(p_o/p)^K \quad ,$$

is derived the following:

$$\bar{\theta}\,(1 + \theta'/\bar{\theta}) = \bar{T}\,(1 + T'/\bar{T})\,(p_o/p)^K$$

$$\bar{\theta} \approx \bar{T}\,(p_o/p)^K \tag{3.1.7}$$

Beginning with the pressure gradient term in Table 3.1,

$$- \frac{1}{\rho} \frac{\partial p}{\partial x_i} \quad ,$$

Applying Equation (3.1.6) gives

$$- R\bar{T} \frac{\partial \ln p}{\partial x_i} \qquad (3.1.8)$$

Taking the logarithmic form of the definition of π (Table 3.2),

$$\ln \pi = \ln c_p + K \left[\ln p - \ln p_o\right] \quad ,$$

differentiating,

$$\frac{\partial \ln \pi}{\partial x_i} = K \frac{\partial \ln p}{\partial x_i} \quad ,$$

and substituting in Equation (3.1.8) gives

$$- \frac{R\bar{T}}{K} \frac{\partial \ln \pi}{\partial x_i} \quad ,$$

or $$- \frac{c_p \bar{T}}{\pi} \frac{\partial \pi}{\partial x_i} \quad ,$$

or $$- \bar{T} (p_o/p)^K \frac{\partial \pi}{\partial x_i} \quad .$$

Finally, substitution of Equation (3.1.7) yields

$$- \bar{\theta} \frac{\partial \pi}{\partial x_i}$$

which is the expression given in Table 3.1. The pressure gradient term has thus been linearized.

Table 3.3. - Preliminary Simplification of Equations

$$\frac{\partial u_i}{\partial t} = u_j \frac{\partial u_i}{\partial x_j} - \overline{\theta} \frac{\partial \pi}{\partial x_i} - g\, \delta_{3i} - \varepsilon_{ijk}\, f_j\, u_k$$

$$\frac{\partial \theta}{\partial t} = - u_j \frac{\partial \theta}{\partial x_j}$$

$$\frac{\partial q}{\partial t} = - u_j \frac{\partial q}{\partial x_j}$$

$$\frac{\partial u_j}{\partial x_j} = 0$$

The next stage in development of the model equations is the derivation of Reynolds equations for the mean variables (see Monin and Yaglom, 1971). It is assumed that

$$u_i = \overline{u_i} + u_i'$$

$$\theta = \overline{\theta} + \theta' \qquad (3.1.9)$$

$$q = \overline{q} + q'$$

$$\pi = \overline{\pi} + \pi'$$

where the mean of a perturbation is zero by definition. Substitution in equations of Table 3.3 and subsequent averaging of the entire equations results in the forms shown in Table 3.4, additional turbulent flux divergence terms being generated by the non-linear advection/convection terms.

Returning briefly to Table 3.3 and examining the vertical equation of motion (i = 3), it can be seen that for mid-latitudes, $f_j \sim 10^{-4}\ s^{-1}$, whereas $g \sim 10\ m.s^{-2}$. Thus, for wind speeds of order $10\ m.s^{-1}$, the Coriolis term will be four orders of magnitude less than g and may be neglected. Haltiner (1971) shows by scale analysis of the vertical equation of motion that a sufficient condition for the hydrostatic approximation is

$$D^2/L^2 << 1 \quad , \qquad (3.1.10)$$

where D is a characteristic vertical scale and L is a characteristic horizontal scale (roughly a quarter wavelength of the disturbances of interest). Postponing until later in this chapter an examination of the limits of validity of the hydrostatic approximation, it will be assumed that the inequality (3.1.10) is satisfied, i.e., the model is hydrostatic, and that, therefore, all terms in the vertical equation of motion except the pressure gradient and gravitational terms are negligible by comparison. In Table 3.5 the hydrostatic equation, derived from the vertical equation of motion (i = 3) is shown separately from the horizontal equations of motion (i = 1, 2).

Table 3.4 - Mean Reynolds Equations

$$\frac{\partial \overline{u_i}}{\partial t} = - \overline{u_j} \frac{\partial \overline{u_i}}{\partial x_j} - \overline{\theta} \frac{\partial \overline{\pi}}{\partial x_i} - g \, \delta_{3i} - \varepsilon_{ijk} \, f_j \, \overline{uk} - \frac{\partial}{\partial x_j} \overline{(u_i' \, u_j')}$$

$$\frac{\partial \overline{\theta}}{\partial t} = - \overline{u_j} \frac{\partial \overline{\theta}}{\partial x_j} - \frac{\partial}{\partial x_j} \overline{(u_j' \, \theta')}$$

$$\frac{\partial \overline{q}}{\partial t} = - \overline{u_j} \frac{\partial \overline{q}}{\partial x_j} - \frac{\partial}{\partial x_j} \overline{(u_j' \, q')}$$

$$\frac{\partial \overline{u_j}}{\partial x_j} = 0$$

Table 3.5 - Closure Assumptions and Hydrostatic Approximation

$$\frac{\partial \overline{u_i}}{\partial t} = -\overline{u_j}\frac{\partial \overline{u_i}}{\partial x_j} - \overline{\theta}\frac{\partial \overline{\pi}}{\partial x_i} - \varepsilon_{ijk} f_j \overline{u_k} + \frac{\partial}{\partial x}\left(K_H \frac{\partial \overline{u_i}}{\partial x}\right) + \frac{\partial}{\partial y}\left(K_H \frac{\partial \overline{u_i}}{\partial y}\right) + \frac{\partial}{\partial z}\left(K_z^{(m)} \frac{\partial \overline{u_i}}{\partial z}\right) \quad , i = 1, 2$$

$$0 = -\overline{\theta}\frac{\partial \overline{\pi}}{\partial x_i} - g \quad , i = 3$$

$$\frac{\partial \overline{\theta}}{\partial t} = -\overline{u_j}\frac{\partial \overline{\theta}}{\partial x_j} + \frac{\partial}{\partial x}\left(K_H \frac{\partial \overline{\theta}}{\partial x}\right) + \frac{\partial}{\partial y}\left(K_H \frac{\partial \overline{\theta}}{\partial y}\right) + \frac{\partial}{\partial z}\left(K_z^{(\theta)} \frac{\partial \overline{\theta}}{\partial z}\right)$$

$$\frac{\partial \overline{q}}{\partial t} = -\overline{u_j}\frac{\partial \overline{q}}{\partial x_j} + \frac{\partial}{\partial x}\left(K_H \frac{\partial \overline{q}}{\partial x}\right) + \frac{\partial}{\partial y}\left(K_H \frac{\partial \overline{q}}{\partial y}\right) + \frac{\partial}{\partial z}\left(K_z^{(q)} \frac{\partial \overline{q}}{\partial z}\right)$$

$$\frac{\partial \overline{u_j}}{\partial x_j} = 0$$

Table 3.6 - Final Governing Equations

$$\frac{\partial u}{\partial t} = - u_j \frac{\partial u}{\partial x_j} - \theta \frac{\partial \pi}{\partial x} + f_3 v - f_2 w + \frac{\partial}{\partial x}\left(K_H \frac{\partial u}{\partial x}\right) + \frac{\partial}{\partial y}\left(K_H \frac{\partial u}{\partial y}\right) + \frac{\partial}{\partial z}\left(K_z^{(m)} \frac{\partial u}{\partial z}\right)$$

$$\frac{\partial v}{\partial t} = - u_j \frac{\partial v}{\partial x_j} - \theta \frac{\partial \pi}{\partial Y} - f_3 u + \frac{\partial}{\partial x}\left(K_H \frac{\partial v}{\partial x}\right) + \frac{\partial}{\partial y}\left(K_H \frac{\partial v}{\partial y}\right) + \frac{\partial}{\partial z}\left(K_z^{(m)} \frac{\partial v}{\partial z}\right)$$

$$\frac{\partial \pi}{\partial z} = - \frac{g}{\theta}$$

$$\frac{\partial \theta}{\partial t} = - u_j \frac{\partial \theta}{\partial x_j} + \frac{\partial}{\partial x}\left(K_H \frac{\partial \theta}{\partial x}\right) + \frac{\partial}{\partial y}\left(K_H \frac{\partial \theta}{\partial y}\right) + \frac{\partial}{\partial z}\left(K_z^{(\theta)} \frac{\partial \theta}{\partial z}\right)$$

$$\frac{\partial q}{\partial t} = - u_j \frac{\partial q}{\partial x_j} + \frac{\partial}{\partial x}\left(K_H \frac{\partial q}{\partial x}\right) + \frac{\partial}{\partial y}\left(K_H \frac{\partial q}{\partial y}\right) + \frac{\partial}{\partial z}\left(K_z^{(q)} \frac{\partial q}{\partial z}\right)$$

$$\frac{\partial w}{\partial z} = - \left(\frac{\partial u}{\partial x} + \frac{\partial v}{\partial y}\right)$$

The next problem is closure of the Reynolds equations. The nature of this problem is summarized concisely by Busch (1973). Without getting involved in a discussion of the possible benefits of higher-order closure at present, it is sufficient to say that first-order closure, specifically K-theory, has been invoked. It has been assumed that

$$-\overline{u_i' u_j'} = \begin{cases} K_H \dfrac{\partial \bar{u}_i}{\partial x_j} & , j = 1, 2 \\ K_z^{(m)} \dfrac{\partial \bar{u}_i}{\partial x_j} & , j = 3 \end{cases} \qquad (3.1.11)$$

$$-\overline{u_j' \theta'} = \begin{cases} K_H \dfrac{\partial \theta}{\partial x_j} & , j = 1, 2 \\ K_z^{(\theta)} \dfrac{\partial \theta}{\partial x_j} & , j = 3 \end{cases} \qquad (3.1.12)$$

$$-\overline{u_j' q'} = \begin{cases} K_H \dfrac{\partial q}{\partial x_j} & , j = 1, 2 \\ K_z^{(q)} \dfrac{\partial q}{\partial x_j} & , j = 3 \end{cases} \qquad (3.1.13)$$

Substitution in Table 3.4 yields equations in Table 3.5.

As a final step, the two horizontal equations of motion are written separately; the hydrostatic approximation and the continuity equations are rearranged to yield diagnostic equations for π and w, respectively and the resulting governing equations are shown in Table 3.6.

3.2. Terrain-Following Coordinate System

The transformed vertical coordinate is:

$$z^* = \bar{s}\left(\frac{z-z_G}{s-z_G}\right) \quad , \tag{3.2.1}$$

where s (x, y, t) is the material surface top of the model, z_G (x, y, t) is the terrain height and $\bar{s}$ is the initial value of s (see Mahrer and Pielke, 1975, 1976). In order to derive the equations in the transformed coordinate system it is necessary to obtain from Equation (3.2.1) the following partial derivatives of z^*:

$$\frac{\partial z^*}{\partial z_G} = \frac{z^*-\bar{s}}{s-z_G} \tag{3.2.2}$$

$$\frac{\partial z^*}{\partial s} = -\frac{z^*}{s-z_G} \tag{3.2.3}$$

$$\frac{\partial z^*}{\partial x} = \frac{\bar{s}}{s-z_G} \quad . \tag{3.2.4}$$

Then, following Phillips (1957), an arbitrary variable, a, is assumed to be a function of the original coordinate system (x, y, z, t). Relations between partial derivatives in that system and those in the transformed system (x', y', z^*, t') are then obtained. It should be noted that x = x', y = y' and t = t'; the primes are required, nevertheless, to distinguish which system is implied when partial derivatives are taken. For example, $\frac{\partial a}{\partial x}$ implies that y, z and t are held constant, whereas $\frac{\partial a}{\partial x'}$, implies that y', z^* and t' are held constant. By the chain rule for partial differentiation:

$$\frac{\partial a}{\partial x} = \frac{\partial a}{\partial x'}\frac{\partial x'}{\partial x} + \frac{\partial a}{\partial y}\frac{\partial y'}{\partial x} + \frac{\partial a}{\partial z^*}\frac{\partial z^*}{\partial x} + \frac{\partial a}{\partial t'}\frac{\partial t'}{\partial x} \tag{3.2.5}$$

Since x' = x, y' = y, t' = t, therefore

$$\frac{\partial x'}{\partial x} = \frac{\partial x}{\partial x} = 1$$

$$\frac{\partial y'}{\partial x} = \frac{\partial y}{\partial x} = 0 \qquad (3.2.6)$$

$$\frac{\partial t'}{\partial x} = \frac{\partial t}{\partial x} = 0$$

Thus Equation (3.2.5) becomes:

$$\frac{\partial a}{\partial x} = \frac{\partial a}{\partial x'} + \frac{\partial a}{\partial z^*} \frac{\partial z^*}{\partial x} \qquad (3.2.7)$$

Similarily,

$$\frac{\partial a}{\partial y} = \frac{\partial a}{\partial y'} + \frac{\partial a}{\partial z^*} \frac{\partial z^*}{\partial y} \quad , \qquad (3.2.8)$$

$$\frac{\partial a}{\partial z} = \frac{\partial a}{\partial z^*} \frac{\partial z^*}{\partial z} \qquad (3.2.9)$$

$$\frac{\partial a}{\partial t} = \frac{\partial a}{\partial t'} + \frac{\partial a}{\partial z^*} \frac{\partial z^*}{\partial t} \qquad (3.2.10)$$

Since z^* is a function of z, s and z_G and the latter two are both functions of x, y and t, the chain rule may again be applied:

$$\frac{\partial z^*}{\partial x} = \frac{\partial z^*}{\partial s} \frac{\partial s}{\partial x} + \frac{\partial z^*}{\partial z_G} \frac{\partial z_G}{\partial x} \quad , \qquad (3.2.11)$$

$$\frac{\partial z^*}{\partial y} = \frac{\partial z^*}{\partial s} \frac{\partial s}{\partial y} + \frac{\partial z^*}{\partial z_G} \frac{\partial z_G}{\partial y} \quad , \qquad (3.2.12)$$

$$\frac{\partial z^*}{\partial t} = \frac{\partial z^*}{\partial s} \frac{\partial s}{\partial t} + \frac{\partial z^*}{\partial z_G} \frac{\partial z_G}{\partial t} \quad . \qquad (3.2.13)$$

Furthermore, since s and z_G are functions of (x', y', t') in the transformed coordinate system, it may be shown that:

$$\frac{\partial s}{\partial x} = \frac{\partial s}{\partial x'}$$

$$\frac{\partial z_G}{\partial x} = \frac{\partial z_G}{\partial x'} \quad , \tag{3.2.14}$$

and similarly for y and t. Thus, substitution of Equation (3.2.14) in Equation (3.2.11), followed by substitution in Equation (3.2.7) yields

$$\frac{\partial a}{\partial x} = \frac{\partial a}{\partial x'} + \frac{\partial a}{\partial z^*}\left[\left(\frac{z^* - \bar{s}}{s - z_G}\right)\frac{\partial z_G}{\partial x'} - \left(\frac{z^*}{s - z_G}\right)\frac{\partial s}{\partial x'}\right] \quad . \tag{3.2.15}$$

Similarly, from Equations (3.2.8), (3.2.9), (3.2.10) are derived

$$\frac{\partial a}{\partial y} = \frac{\partial a}{\partial y'} + \frac{\partial a}{\partial z^*}\left[\left(\frac{z^* - \bar{s}}{s - z_G}\right)\frac{\partial z_G}{\partial y'} - \left(\frac{z^*}{s - z_G}\right)\frac{\partial s}{\partial y'}\right] \quad , \tag{3.2.16}$$

$$\frac{\partial a}{\partial z} = \frac{\partial a}{\partial z^*}\frac{\bar{s}}{s - z_G} \quad , \tag{3.2.17}$$

$$\frac{\partial a}{\partial t} = \frac{\partial a}{\partial t'} + \frac{\partial a}{\partial z^*}\left[\left(\frac{z^* - \bar{s}}{s - z_G}\right)\frac{\partial z_G}{\partial t'} - \left(\frac{z^*}{s - z_G}\right)\frac{\partial s}{\partial t'}\right] \quad . \tag{3.2.18}$$

It is useful to derive a vertical motion, w^*, in the transformed coordinate system by defining

$$\frac{da}{dt'} = \frac{\partial a}{\partial t'} + u\frac{\partial a}{\partial x'} + v\frac{\partial a}{\partial y'} + w^*\frac{\partial a}{\partial z^*} \tag{3.2.19}$$

and noting that

$$\frac{da}{dt'} = \frac{da}{dt} = \frac{\partial a}{\partial t} + u\frac{\partial a}{\partial x} + v\frac{\partial a}{\partial y} + w\frac{\partial a}{\partial z} \quad . \tag{3.2.20}$$

Substitution of Equation (3.2.19) for the left-hand-side of (3.2.20) and Equations (3.2.15) to (3.2.18) for the right-hand-side yields:

$$w^* = \frac{\bar{s}}{s-z_G} w + \left(\frac{z^*-\bar{s}}{s-z_G}\right)\left(\frac{\partial z_G}{\partial t'} + u\frac{\partial z_G}{\partial x'} + v\frac{\partial z_G}{\partial y'}\right) - \left(\frac{z^*}{s-z_G}\right)\left(\frac{\partial s}{\partial t'} + u\frac{\partial s}{\partial x'} + v\frac{\partial s}{\partial y'}\right) \qquad (3.2.21)$$

It should be noted that the term $\frac{\partial z_G}{\partial t'}$ is retained in Equation (3.2.21) because, during initialization of the model, the topography is added gradually over a period of, say, 30 min of integration time. Thereafter the term would be zero.

Application of Equations (3.2.15) to (3.2.17) to the pressure gradient terms in Table 3.6 produces the following results:

$$\theta\frac{\partial \pi}{\partial x} = \theta\frac{\partial \pi}{\partial x'} + \theta\frac{\partial \pi^*}{\partial z}\left[\left(\frac{z^*-\bar{s}}{s-z_G}\right)\frac{\partial z_G}{\partial x'} - \left(\frac{z^*}{s-z_G}\right)\frac{\partial s}{\partial x'}\right], \qquad (3.2.22)$$

$$\theta\frac{\partial \pi}{\partial y} = \theta\frac{\partial \pi}{\partial y'} + \theta\frac{\partial \pi^*}{\partial z}\left[\left(\frac{z^*-\bar{s}}{s-z_G}\right)\frac{\partial z_G}{\partial y'} - \left(\frac{z^*}{s-z_G}\right)\frac{\partial s}{\partial y'}\right], \qquad (3.2.23)$$

$$\frac{\partial \pi}{\partial z} = \frac{\partial \pi^*}{\partial z}\left(\frac{\bar{s}}{s-z_G}\right). \qquad (3.2.24)$$

Incorporating the hydrostatic approximation (Table 3.6) yields

$$\theta\frac{\partial \pi}{\partial x} = \theta\frac{\partial \pi}{\partial x'} - g\left[\left(\frac{z^*-\bar{s}}{\bar{s}}\right)\frac{\partial z_G}{\partial x'} - \frac{z^*}{\bar{s}}\frac{\partial s}{\partial x'}\right], \qquad (3.2.25)$$

$$\theta\frac{\partial \pi}{\partial y} = \theta\frac{\partial \pi}{\partial y'} - g\left[\left(\frac{z^*-\bar{s}}{\bar{s}}\right)\frac{\partial z_G}{\partial y'} - \frac{z^*}{\bar{s}}\frac{\partial s}{\partial y'}\right], \qquad (3.2.26)$$

$$\frac{\partial \pi^*}{\partial z} = -\left(\frac{s-z_G}{\bar{s}}\right)\frac{g}{\theta}. \qquad (3.2.27)$$

Regarding the horizontal eddy diffusion terms, it may be assumed that

$$\frac{\partial}{\partial x}\left(K_H \frac{\partial u}{\partial x}\right) = \frac{\partial}{\partial x'}\left(K_H' \frac{\partial u}{\partial x'}\right) \tag{3.2.28}$$

and similarly for y in place of x and v, θ or q in place of u, where

$$K_H' = \alpha\,(\Delta x')\,(\Delta y')\left\{\left(\frac{\partial v}{\partial x'} + \frac{\partial u}{\partial y'}\right)^2 + \frac{1}{2}\left[\left(\frac{\partial u}{\partial x'}\right)^2 + \left(\frac{\partial v}{\partial y'}\right)^2\right]\right\}^{1/2} \tag{3.2.29}$$

and K_H is defined in the same way but without primes.

For the vertical eddy diffusion terms, K_z is a function of a dimensionless height so that change of the vertical coordinate does not introduce changes in K_z itself, except for replacement of z by z^*, etc. The vertical derivatives, however, are responsible for the introduction of a multiplying factor due to double application of Equation (3.2.9). Thus

$$\frac{\partial}{\partial z}\left(K_z^{(m)} \frac{\partial u}{\partial z}\right) = \left(\frac{\bar{s}}{s-z_G}\right)^2 \frac{\partial}{\partial z^*}\left(K_z^{(m)} \frac{\partial u}{\partial z^*}\right) \quad , \tag{3.2.30}$$

where

$$K_z(z^*) = \begin{cases} K_z(z_i) + \left(\dfrac{z_i - z^*}{z_i - h}\right)^2 \left\{K_z(h) - K_z(z_i) + (z^* - h)\left[\left.\dfrac{\partial K_z}{\partial z^*}\right|_h + 2\,\dfrac{K_z(h) - K_z(z_i)}{z_i - h}\right]\right\}, & h < z^* < z_i \\ K_z(z_i) \quad , \quad z_i < z^* \\ \dfrac{z^*}{h}\,K_z(h) \quad , \quad z^* < h \end{cases} \tag{3.2.31}$$

and similarly for v, θ and q.

Table 3.7 - Governing Equations in Terrain-Following Coordinate System

$$\frac{\partial u}{\partial t} = - u \frac{\partial u}{\partial x} - v \frac{\partial u}{\partial y} - w^* \frac{\partial u}{\partial z^*} - \theta \frac{\partial \pi}{\partial x} + g \left[\left(\frac{z^* - \bar{s}}{\bar{s}} \right) \frac{\partial z_G}{\partial x} - \frac{z^*}{\bar{s}} \frac{\partial s}{\partial x} \right] + f_3 v - f_2 w$$

$$+ \frac{\partial}{\partial x} \left(K_H \frac{\partial u}{\partial x} \right) + \frac{\partial}{\partial y} \left(K_H \frac{\partial u}{\partial y} \right) + \left(\frac{\bar{s}}{s - z_G} \right)^2 \frac{\partial}{\partial z^*} \left(K_z^{(m)} \frac{\partial u}{\partial z^*} \right)$$

$$\frac{\partial v}{\partial t} = - u \frac{\partial v}{\partial x} - v \frac{\partial v}{\partial y} - w^* \frac{\partial v}{\partial z^*} - \theta \frac{\partial \pi}{\partial y} + g \left[\left(\frac{z^* - \bar{s}}{\bar{s}} \right) \frac{\partial z_G}{\partial y} - \frac{z^*}{\bar{s}} \frac{\partial s}{\partial y} \right] - f_3 u$$

$$+ \frac{\partial}{\partial x} \left(K_H \frac{\partial v}{\partial x} \right) + \frac{\partial}{\partial y} \left(K_H \frac{\partial v}{\partial y} \right) + \left(\frac{\bar{s}}{s - z_G} \right)^2 \frac{\partial}{\partial z^*} \left(K_z^{(m)} \frac{\partial v}{\partial z^*} \right)$$

$$\frac{\partial \pi}{\partial z} = - \left(\frac{s - z_G}{\bar{s}} \right) \frac{g}{\theta}$$

$$\frac{\partial \theta}{\partial t} = - u \frac{\partial \theta}{\partial x} - v \frac{\partial \theta}{\partial y} - w^* \frac{\partial \theta}{\partial z^*}$$

$$+ \frac{\partial}{\partial x} \left(K_H \frac{\partial}{\partial x} \right) + \frac{\partial}{\partial y} \left(K_H \frac{\partial}{\partial y} \right) + \left(\frac{\bar{s}}{s - z_G} \right)^2 \frac{\partial}{\partial z^*} \left(K_z^{(\theta)} \frac{\partial \theta}{\partial z^*} \right)$$

$$\frac{\partial q}{\partial t} = - u \frac{\partial q}{\partial x} - v \frac{\partial q}{\partial y} - w^* \frac{\partial q}{\partial z^*}$$

$$+ \frac{\partial}{\partial x} \left(K_H \frac{\partial q}{\partial x} \right) + \frac{\partial}{\partial y} \left(K_H \frac{\partial q}{\partial y} \right) + \left(\frac{\bar{s}}{s - z_G} \right)^2 \frac{\partial}{\partial z^*} \left(K_z^{(q)} \frac{\partial q}{\partial z^*} \right)$$

$$\frac{\partial w^*}{\partial z^*} = - \left(\frac{\partial u}{\partial x} + \frac{\partial v}{\partial y} \right) + \frac{1}{s - z_G} \left(\frac{\partial z_G}{\partial t} + u \frac{\partial z_G}{\partial x} + v \frac{\partial z_G}{\partial y} \right) - \frac{1}{s - z_G} \left(\frac{\partial s}{\partial t} + u \frac{\partial s}{\partial x} + v \frac{\partial s}{\partial y} \right)$$

Finally, application of Equations (3.2.15), (3,2.16), (3.2.17) and (3.2.21) enable transformation of the continuity equation.

All the transformed equations are shown in Table 3.7 where primes have been dropped for convenience, although the asterix is retained on z.

3.3. Auxiliary Equations and Boundary Conditions

Table 3.7 consists of six equations (four prognostic, two diagnostic) in the unknown variables, u, v, w_*, π, θ, q. The terrain-following coordinate system, however, introduced an additional unknown, s. Furthermore, the vertical eddy diffusion coefficient is dependent on z_i, the planetary boundary layer height (see Equation (3.2.31)). Thus, equations for s and z_i are required.

The former is obtained by integrating the continuity equation from $z^* = 0$ to $z^* = \bar{s}$, putting $w_* = 0$ at top and bottom. The resulting prognostic equation is:

$$\frac{\partial s}{\partial t} = \frac{\partial z_G}{\partial t} - \frac{1}{\bar{s}} \int_0^{\bar{s}} \left\{ \frac{\partial}{\partial x} \left[u(s-z_G) \right] + \frac{\partial}{\partial y} \left[v(s-z_G) \right] \right\} dz^* \quad , \tag{3.3.1}$$

where the first term is only required during the early stages of model integration as the terrain is growing.

The prognostic equation for the boundary layer height, z_i, follows Deardorff (1974):

$$\frac{\partial z_i}{\partial t} = -u \frac{\partial z_i}{\partial x} - v \frac{\partial z_i}{\partial y} + w_i + \frac{1.8 \left[W_*^3 + 1.1\, u_*^3 - 3.3\, u_*^2\, f_3\, z_i \right]}{g \frac{z_i^2}{\theta_s} \frac{\partial \theta^+}{\partial z} + 9\, W_*^2 + 7.2\, u_*^2}$$

where

$$W_* = \begin{cases} \left(-\frac{g}{\theta_s}\, u_*\, \theta_*\, z_* \right)^{1/3} , & \theta_* \leq 0 \\ 0 , & \theta > 0 \quad , \end{cases} \tag{3.3.3}$$

θ_s is the potential temperature at the surface, $\frac{\partial \theta^+}{\partial z}$ is the potential temperature gradient immediately above the planetary boundary layer and w_i is the synoptic-scale vertical velocity at the top of the planetary boundary layer. The other symbols have their usual definitions.

The hydrostatic equation is integrated downwards from $z^* = \bar{s}$ in order to obtain π. Thus values of $\pi(t)$ at $z^* = \bar{s}$ are required. These are determined from

$$\pi\ (s,\ t) = \pi\ (\bar{s},\ 0) - \frac{g}{\bar{\theta}}\ (s - \bar{s}) \tag{3.3.4}$$

where $\bar{\theta}$ is the vertical mean potential temperature in the layer between s and $\bar{s}$.

The value of K_z at the top of the surface layer (see Equation 3.2.31) is given by

$$K_z^{\ m}\ (h) = \frac{\kappa\ u_*\ h}{\phi_m\ (\zeta)}$$

$$K_z^{\ (\theta)}\ (h) = \frac{\kappa\ u_*\ h}{\phi_\theta\ (\zeta)} \tag{3.3.5}$$

$$K_z^{\ (q)}\ (h) = \frac{\kappa\ u_*\ h}{\phi_q\ (\zeta)}$$

where $h = z_i/25$, $\zeta = z_*/L$ and

$$L = \frac{\theta\ u_*^{\ 2}}{\kappa\ g\ \theta_*} \tag{3.3.6}$$

is the Monin-Obukhov Length. In Equations (3.3.5) the dimensionless velocity, temperature and humidity gradients ϕ_m, ϕ_θ, ϕ_q are from Yamamoto and Shimanuki (1966). The value of $K_z\ (z_i)$ in Equation (3.2.31) is assumed to be 1 $cm^{\ 2}.s^{-1}$.

Surface roughness length is taken to be 4 cm over land and

$$z_o = 0.032\ u_*^{\ 2}/g \tag{3.3.7}$$

$$z_o \geq 0.0015\ cm$$

over water (Clarke, 1970).

The values of u_* and θ_* are determined iteratively from

$$u_* = \frac{\kappa\,(u^2+v^2)^{1/2}}{G_i(|\zeta|) - G_i(|\zeta_o|)} \tag{3.3.8}$$

$$\theta_* = \frac{\kappa\,\left(\theta-\theta(z_o)\right)}{G_i(|\zeta|) - G_i(|\zeta_o|)} \tag{3.3.9}$$

where $\zeta_o = z_o/L$ and G_i is a profile function ($i = 1, 2$ implies unstable and stable stratifications, respectively).

At $z^* = 0$ the boundary conditions are

$$u = v = w^* = 0$$

$$q = \text{constant}$$

$$\theta = \begin{cases} \text{constant over water} \\ \text{specified as a function (Fourier Series) of time over land} \end{cases}$$

At $z^* = \bar{s}$:

$$u = u_g$$

$$v = v_g$$

$$w^* = 0$$

π is determined from Equation (3.3.4)

θ = constant.

At the lateral boundaries:

$$w^* = \frac{\partial s}{\partial t} = \frac{\partial \theta}{\partial x} = \frac{\partial q}{\partial x} = \frac{\partial \pi}{\partial x} = 0 \qquad \text{on x boundaries}$$

$$w^* = \frac{\partial s}{\partial t} = \frac{\partial \theta}{\partial y} = \frac{\partial q}{\partial y} = \frac{\partial \pi}{\partial y} = 0 \qquad \text{on y boundaries}$$

$$\frac{\partial u}{\partial x} = \frac{\partial v}{\partial x} = 0 \qquad \text{on x - outflow boundaries}$$

$$\frac{\partial u}{\partial y} = \frac{\partial v}{\partial y} = 0 \qquad \text{on y - outflow boundaries}$$

u = constant, v = constant on inflow boundaries.

For initial conditions, surface values of pressure, temperature and humidity are specified. The geostrophic wind is specified. The winds are obtained by integrating the system

$$\frac{\partial u}{\partial t} = f_3 \left(v - v_g\right) + \frac{\partial}{\partial z}\left(K_z^{(m)} \frac{\partial u}{\partial z}\right) \tag{3.3.10}$$

$$\frac{\partial v}{\partial t} = - f_3 \left(u - u_g\right) + \frac{\partial}{\partial z}\left(K_z^{(m)} \frac{\partial v}{\partial z}\right)$$

for six inertial periods.

3.4. Numerical Techniques

The equations are integrated forward in time using a semi-implicit scheme (see Richtmyer and Morton, 1967; for an application to the primitive equations see Kwizak and Robert, 1971). Upstream finite differencing is employed to approximate horizontal derivates. The model grid mesh is staggered with u, v and π defined on the grid points, θ and q defined on levels above and below the main grid levels and w defined on the main grid levels but at the centers of the squares formed by four grid points. In order to maintain linear computational stability the u and v equations are evaluated first, the w equation second (along with the equation for the height of the material surface), followed by equations for θ, q and π.

In order to describe the semi-implicit time integration scheme it is first necessary to examine the method of evaluating vertical eddy diffusion terms. If the u equation in Table 3.7 is considered, it is seen that vertical eddy diffusion is given exactly as

$$\left(\frac{\bar{s}}{s-z_G}\right)^2 \frac{\partial}{\partial z^*}\left(K_z^{(m)} \frac{\partial u_*}{\partial z}\right)$$

Letting the subscripts j, j+1, j-1 represent a grid level, the grid level above and the grid level below, respectively and $j+\frac{1}{2}$, $j-\frac{1}{2}$ represent the staggered grid levels immediately above and below level j on which the eddy coefficients are defined, then the eddy diffusion term is approximated as follows

$$\left(\frac{\bar{s}}{s-z_G}\right)^2 \left(\frac{1}{\Delta Z_T}\right)\left[\frac{K_{j+\frac{1}{2}}}{\Delta Z_1}\left(u_{j+1}^n - u_j^{n+1}\right) - \frac{K_{j-\frac{1}{2}}}{\Delta Z_2}\left(u_j^{n+1} - u_{j-1}^n\right)\right]$$

where

$$\Delta Z_T = z^*_{j+\frac{1}{2}} - z^*_{j-\frac{1}{2}} \quad ,$$

$$\Delta Z_1 = z^*_{j+1} - z^*_j \quad ,$$

$$\Delta Z_2 = z^*_j - z^*_{j-1} \quad ,$$

and the superscripts n and n+1 represent values at the current and subsequent (one timestep later) times, respectively.

The presence of the u_j^{n+1} values in the right-hand-side of the u equation, makes the scheme for solving this equation implicit. Fortunately, however, the u_j^{n+1} term appears in a linear sense and thus it can easily be moved to the left-hand-side of the equation. Mahrer and Pielke (1976) refer to the finite difference representation of the vertical diffusion as a Dufort-Frankel scheme. This is not completely true, although there are similarities (see Richtmyer and Morton, 1967). The Dufort-Frankel scheme, in fact, uses three time-levels, not two. Nevertheless, the idea of moving the u_j^{n+1} term to the left-hand-side is the same as in the Dufort-Frankel scheme (see also Walmsley, 1976). When this is done, the u equation may be expressed in finite difference form as follows:

$$u_j^{n+1} = u_j^n + \Delta t \left(\frac{\bar{s}}{s-z_G}\right)^2 \left(\frac{1}{\Delta Z_T}\right) \left[\frac{K_{j+\frac{1}{2}}}{\Delta Z_1} u_{j+1}^n + \frac{K_{j-\frac{1}{2}}}{\Delta Z_2} u_{j-1}^n\right] + \text{other terms}$$

$$\overline{\qquad\qquad\qquad\qquad\qquad\qquad\qquad\qquad\qquad\qquad\qquad\qquad\qquad\qquad\qquad\qquad}$$

$$1 + \Delta t \left(\frac{\bar{s}}{s-z_G}\right)^2 \frac{1}{\Delta Z_T} \left[\frac{K_{j+\frac{1}{2}}}{\Delta Z_1} + \frac{K_{j-\frac{1}{2}}}{\Delta Z_2}\right] \qquad (3.4.1)$$

where the second term in the denominator originated from the u_j^{n+1} terms in the diffusion term. The v, θ and q equations are treated in a similar manner.

As mentioned previously, the topography is allowed to grow linearly with time during the first 30 minutes of model integration. This technique helps to avoid numerical instabilities. Thereafter a further 3.5 hr. of integration are carried out in order to allow the model to approach a steady-state before actual experiments are begun. In all experiments described in subsequent chapters of this report, 11 vertical levels (50, 100, 300, 600, 1000, 1400, 2100, 3000, 4000 5000, 6000 m) were employed. The horizontal grid spacing was 5 km with 18 grid points in the direction cross-wind to the geostrophic wind and 15 grid points in the longitudinal direction with an additional 3 grid points at each longitudinal boundary spaced 10, 15 and 20 km apart, respectively.

3.5. Deficiencies in the Model

The assumption made in Equation (3.1.10) is a sufficient condition for the hydrostatic approximation. This assumption suggests that the present model may not be valid for sufficiently small horizontal scales. However, the hydrostatic assumption is valid for scales considered here and perhaps even to scales about half an order of magnitude smaller. Changing to an anelastic condition, therefore, should not be considered a priority when improvements to the model are contemplated.

The method of initializing both land and water surfaces with respect to a roughness length appropriate to water was responsible for generating inertial oscillations in the results. Improvements were made in this area as described later in the present report.

The vertical grid spacing is somewhat arbitrary, a feature which ignores the advice of Taylor and Delage (1971) who argue that a proper coordinate transformation can avoid unnecessary truncation error in the finite difference approximation to vertical derivatives.

The upstream differencing scheme employed for approximating horizontal derivatives in this model, although contributing to computational stability, is known to be computationally diffusive. It is possible that such artifical diffusion can even mask the explicit horizontal diffusion incorporated in the formulation of the model. Closely linked to the horizontal differencing scheme is the method of specifying boundary conditions on the lateral and longitudinal boundaries. Experience shows that the results are quite sensitive to boundary conditions.

The development of complex models of atmospheric motion is often carried out with the simple specification of surface temperature substituted for a surface energy budget. Great effort is exerted in attempting to properly represent the atmospheric dynamics and relevant physics in the numerical model but proper handling of the surface energy exchanges is postponed. The present model is no exception. Incorporation of an energy budget that enables the surface temperature to be calculated with sufficient accuracy is not a simple matter; nevertheless it should be attempted.

Finally, as an optional feature, the model should calculate kinetic and available potential energy budgets and exchanges of energy from one form to another. This facility would aid in the diagnosis of model behaviour and analysis of results. A first step has been made to calculate an approximate kinetic energy budget.

CHAPTER IV

DEVELOPMENT AND TESTS OF THE MODEL

4.1. Preliminary Program Modification

The model described in the previous chapter was made available to the current authors in May 1976 in a form coded for the computer at the National Center for Atmospheric Research (NCAR). The version of the model obtained had not been extensively tested, although it was a refinement of previous model versions.

The first task which had to be undertaken was to modify the code to operate in the AES CYBER 76 environment. The NCAR version, because of the special features of that machine, did not initially run on the AES machine. Conversion proved to be rather straightforward. Different formats for disk-core fast data transfers proved to be the major concern.

Initial tests of the model uncovered a number of errors and inconsistencies. Specifically:

(a) Omission of a COMMON statement with the effect that thermal wind was zero in the calculations.

(b) Omission of a factor two in one of the surface layer profile function formulations.

(c) Occasional incorrect keypunching of variable names in the surface layer profile function formulation.

(d) Implicit specification of the lower boundary as water and consequent omission of land roughness and temperature where appropriate.

(e) Incorrect special handling of lateral boundaries for the total domain depth calculation.

These were corrected in consultation with Prof. W.L. Cotton at Colorado State University who was simultaneously investigating this code.

Considerable effort was expended in improving the efficiency and generality of the coding. In particular maximum advantage was made of the AES CYBER directly addressable Large Core Memory not available at NCAR. This effort resulted in a 40% saving in execution time. After implementing these improvements, using a 20 x 18 x 11 grid, each timestep occupied 0.81 seconds of computer time or about 2 minutes for each simulated hour.

It soon became evident that with simulations several hours long, delays occurred in computer processing. Long jobs such as this are only run during the night and operators seemed reluctant to run them at all on some occasions. In the most extreme case a one week delay was encountered. This deplorable situation was alleviated by restructuring the program to take advantage of the DEVOUR facility on the CYBER. With DEVOUR a long job is submitted as a series of short jobs, automatically, one on completion of the previous. The three week effort involved in implementing DEVOUR operation was more than repaid in faster turnaround. In many cases several hours simulation were achieved during normal working hours.

4.2. Initialization

The NCAR version of this model employed an observed vertical mass distribution and specified geostrophic and thermal winds for initialization. As explained in the previous chapter the boundary layer initial winds were derived from the prognostic Ekman equations (3.3.10) applied over a water surface. The assumption of a water surface was reasonable for the initial application of the model to airflow over and around south Florida. However, for simulations over a primarily land surface it is inappropriate to initialize with water roughness. Where the surface roughness and wind profile are incompatible the wind solution evolves through damped inertial oscillations as evident for Case B in Fig. 4.1. This should be compared with the evolution for Case A in which the initialization roughness is compatible with the underlying value. The small residual oscillation for case A is the result of incomplete convergence of the initialization and imposed inhomogeniety in surface characteristics downwind of the location in question.

Choice of a best initialization depends upon the nature of the investigation. For short-range forecasting purposes the exact initial conditions will be important and need to be defined well from observation. For longer range forecast problems the nature of diabatic forcings can play a dominant role governing atmospheric evolution. Exact specification of initial atmospheric conditions may not be as important. In simulation modelling the purpose is not to investigate evolution of a specific meteorological situation but rather to gain insight into the physics of the evolution of a class of situations. If, for example, a particular diabatic forcing was of interest (say a sea-breeze situation), a relaxed specification of initial atmospheric conditions might be appropriate. Essentially an initial condition which might reasonably be expected to occur would be appropriate. This is advantageous to the simulation modeller in that the initialization task is less demanding.

The above consideration is illustrated in Fig. 4.1 which shows the hour-by-hour evolution of wind at the first grid point above the surface for heated and unheated cases with different initializations. The polar plot is of the wind vector deviations from the unheated equilibrium value. Heating for Cases C and D commences at hour four. Small discrepancies between heated and unheated cases with similar initializations will be noted because of a slightly altered upper boundary stability imposed. The important point to note is that the two heated cases with different initializations follow similar evolutions after hour four, quite distinct from the evolution of the unheated cases. Additional tests such as this indicate that with commonly found diabatic surface forcings the qualitative nature of the evolution was independent of any reasonable initialization.

Based on the above considerations an initialization scheme was adopted where wind was initialized to be in Ekman balance with the underlying surface and then the equations integrated forward for a few hours to permit adjustments to advective effects.

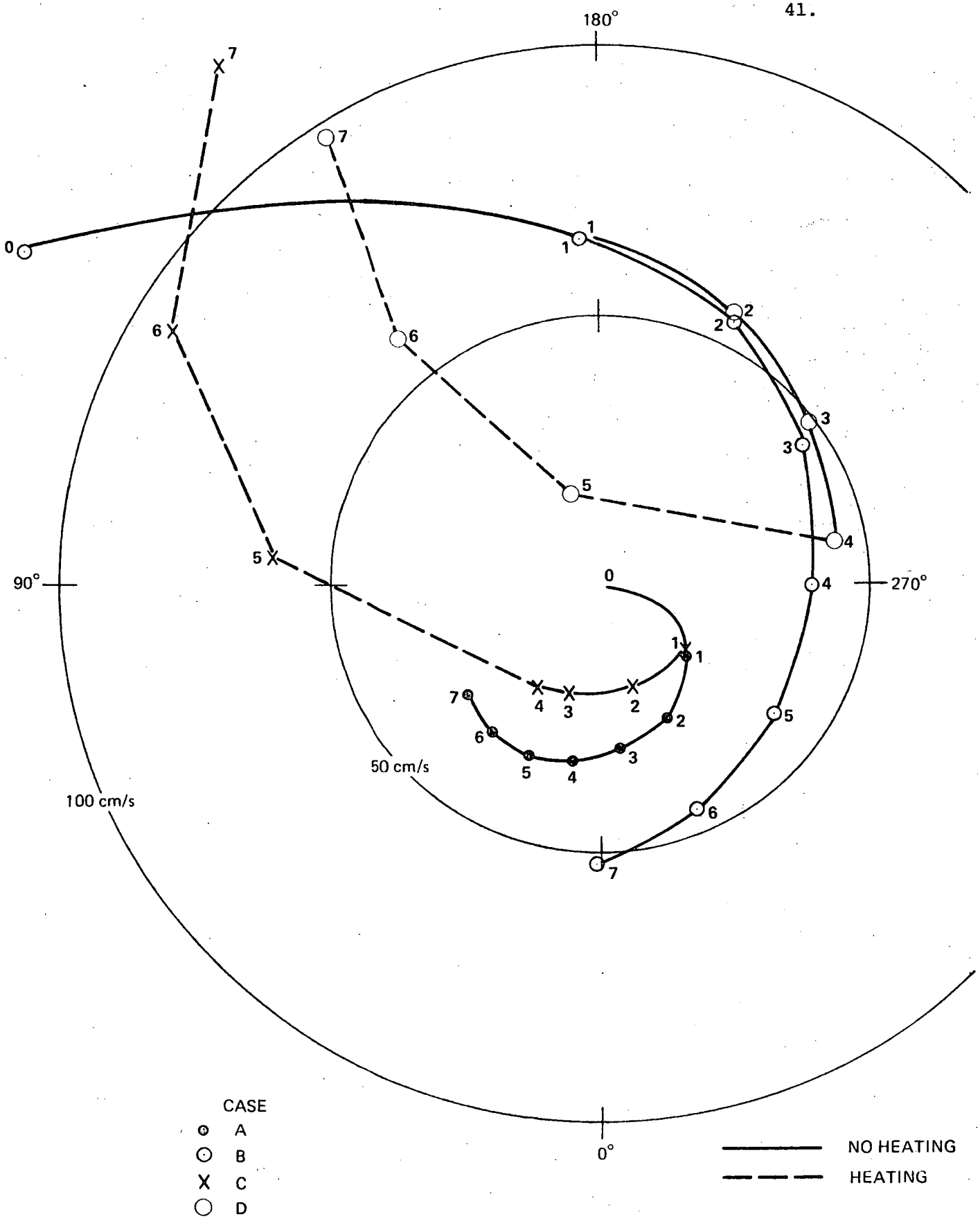

Figure 4.1 Hourly Vector Deviations of Wind Velocity from Equilibrium Values over Land.

4.3. Boundary Conditions

Difficulties were encountered with the u and v boundary conditions (see Section 3.3) in early experiments with the model. The problems occurred when a double flow reversal occurred at a boundary in such a way that first inflow, then outflow, then inflow conditions prevailed during the course of the time integration. In the first phase, boundary conditions remained fixed at their initial values (i.e., the synoptic background values). After the first flow reversal, outflow conditions existed and values of u and v were allowed to change with time in accordance with the zero-derivative condition. Conditions at the boundaries could, therefore, deviate significantly from synoptic values without having harmful effects on the model interior. As soon as a second flow reversal took place, however, the boundary conditions were again fixed, not at synoptic values, but at the last values attained during the outflow phase. Thus unrealistic values were advected into the model domain from the boundary, causing very rapid degradation of the solution. In order to avoid this problem a temporary solution of applying the zero-derivative condition for u and v at all lateral boundaries regardless of flow direction was implemented. Effort was then concentrated on other aspects of the model, the boundary conditions at least temporarily under control.

After examination of results from an idealized ridge experiment, however, it was realized that the zero-derivative condition was not satisfactory. In this experiment an analytic "Witch of Agnesi" ridge of height 100 m, width 30 km at half-height, aligned in a direction perpendicular to the geostrophic wind, was investigated. The airflow was initially in balance over uniform terrain with a neutral temperature stratification and geostrophic wind speed of $10\ m.s^{-1}$. The ridge was allowed to grow to its full height during the first 30 min of integration. A timestep of 30 s was employed, although tests with a 20 s timestep indicated no significant change in the results. No surface heating was incorporated, so the surface potential temperature was held constant.

Figure 4.2 displays the evolution of pseudo-total kinetic energy (the sum of the squares of the horizontal wind speed at all grid points). During the first six hours of integration with the zero-derivative condition, the kinetic energy remained within 10% of its initial value (despite the effects of terrain-growing). Thereafter it increased rapidly so that after nine hours it was about 38% larger than its initial value. It is evident that the model results were very gradually becoming unrealistic. Wind speeds, for example, attained values near geostrophic over most of the domain (the pseudo-total kinetic energy for a uniform wind speed of 10 $m.s^{-1}$ would be approximately 420 J/g, just slightly more than the actual value reached at hour nine).

Further tests of the boundary conditions for the same idealized ridge topography were evidently required. It was felt with this particular terrain that the longitudinal boundaries (upwind and downwind with respect to the geostrophic wind) should not present difficulties since the terrain height gradually approached zero there. Accordingly, the longitudinal boundary conditions were restored to their original state (see Section 3.3; zero-derivative if outflow, constant if inflow). At the lateral boundaries, on the other hand, the terrain, rising to a maximum of 100 m, extended right to the boundaries. This seemed to be a likely source of difficulties. Hence it was decided to run an experiment with the ridge effectively extending to infinity in both directions. This was accomplished by applying periodic or cyclic boundary conditions on the lateral boundaries. The results of this experiment, also shown in Fig. 4.2, are much more satisfactory, at least in terms of the pseudo-total kinetic energy which at nine hours is only about 5% greater than its initial value.

It may be concluded from the experiments described above that considerable attention must be drawn to the boundary conditions, particularly in cases where topographic features are close to the boundaries. Additionally, the terrain features may have to be considerably damped near the boundaries.

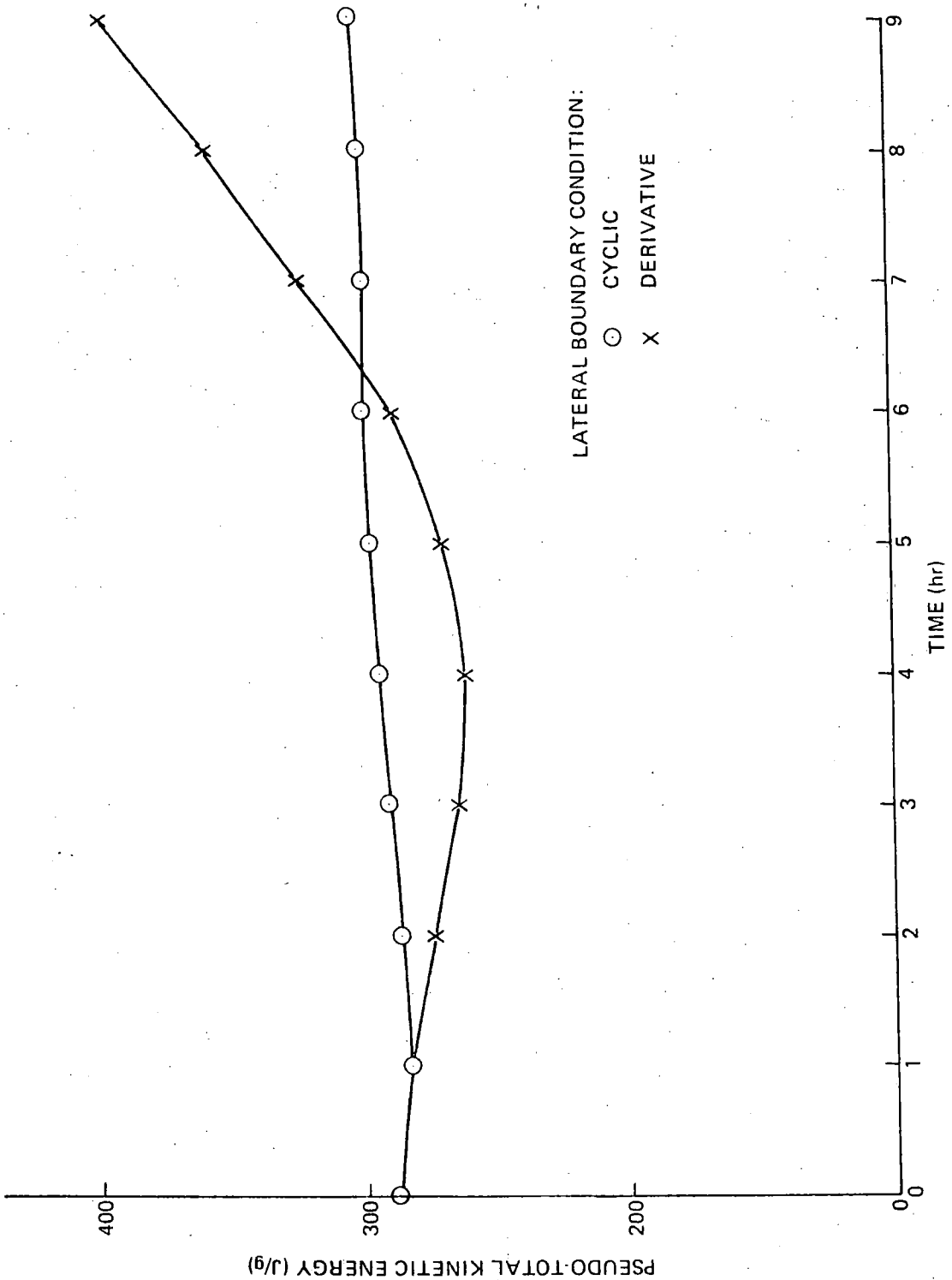

Figure 4.2. Pseudo- Kinetic Energy Evolution for Analytic Ridge Case Studies with Different Lateral Boundary Conditions.

It seems, however, that the method of specification of the boundary conditions is closely coupled to the method of horizontal finite differencing employed. It is planned to investigate alternatives to the upstream differencing scheme which is presently used. Boundary conditions should be examined at the same time.

4.4. Idealized Lake Breeze Experiment

A numerical experiment was performed with the mesoscale model in order to simulate an idealized coastal situation. A straight coastline approximately through the middle of the model domain was specified to be aligned to the geostrophic wind. The land was assumed to have zero elevation everywhere and was located to the right with respect to the geostrophic wind direction. Thus (with the assumption of a latitude for Toronto of 43.5°N, i.e., $f_3 = +1.00 \times 10^{4}$) the low level equilibrium Ekman flow would have a component from land to lake. More specifically, the geostrophic flow was assumed to be easterly (90°), the land was to the north of an east-west shoreline and initial wind directions at the lowest grid level (50 m) were approximately 80°. Heating was begun after four hours of integration (at 8:00 a.m. L.S.T.) having an amplitude of 6°C which is reached approximately 8-9 hours after the commencement of heating. (It should be noted that the arbitrarily chosen L.S.T. time scale is perhaps about 2 hours late compared with an average summer day).

Wind direction and vertical wind speed results are shown in Fig. 4.3. The time scale on the abscissa begins at the time of commencement of heating, 4 hours after the start of integration or at an assumed time of 8:00 a.m. L.S.T. The lake breeze begins at about 10:20 a.m., the wind direction continuing to shift thereafter until between 1:00 and 2:00 p.m. a direction of about 120° is achieved. This shift represents a veer of more than 40° from the equilibrium unheated situation. These wind direction changes are accompanied by weak subsidence over the water and somewhat stronger upward vertical motion over land, reaching a maximum in excess of 1.5 cm. s^{-1} at about 2:30 p.m. This experiment was terminated at 3:00 p.m., approximately 1.5 hours before the time of maximum surface temperature. During the period that was examined, however, the lake-breeze was seen to penetrate inland about 20 km against an adverse equilibrium unheated surface flow oriented at more than 10° to the shoreline.

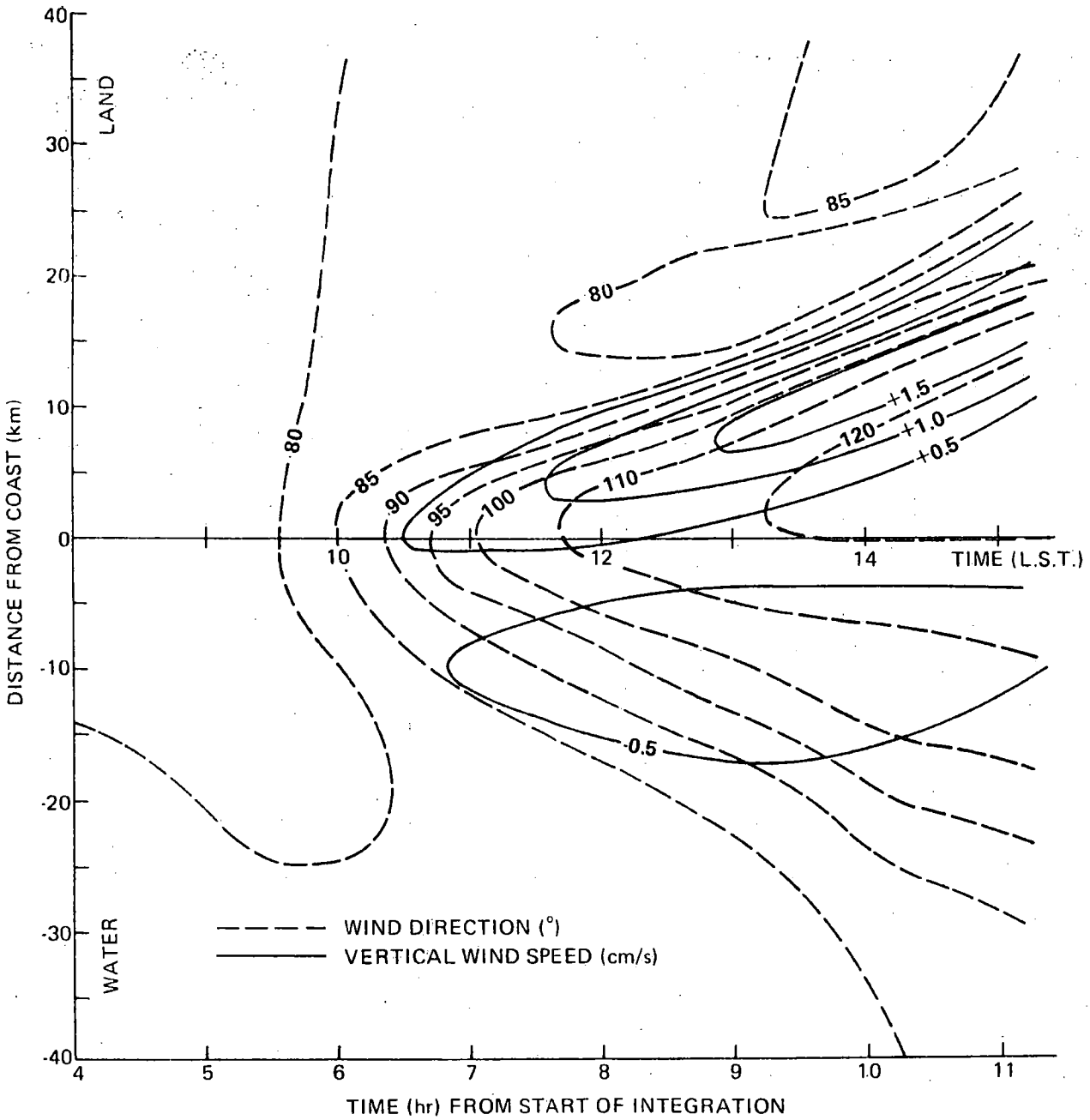

Figure 4.3. Evolution of Wind Direction and Vertical Wind Speed at 50 m for the Lake Breeze Experiment.

This lake-breeze case study illustrates that the model is capable of reasonably simulating atmospheric flow phenomena important for air quality. There is good qualitative and surprisingly good quantitative agreement with the study by Estoque et al. (1976). In the following chapter the implications of this case study to air quality in a lakeshore case are investigated.

CHAPTER V

APPLICATION TO AIR QUALITY STUDIES

As noted in previous chapters, the model under investigation has numerous deficiencies which need to be rectified. Despite these shortcomings there is useful qualitative information applicable to air quality studies to be gathered from investigations with the model "as is". In this chapter mesoscale air pollution trajectories for the simple North Coast lake-breeze simulation presented in the previous chapter are calculated. The case study illustrates how even a simple simulation can lead to important insights regarding the role of mesoscale processes in air pollution dispersion. Their importance is documented in a recent observational study by Lyons and Cole (1976) which gives complementary evidence that the lake-breeze is a major factor in the long-range transport of pollution (ozone) from sources in Chicago to Milwaukee 100 km distant. Milwaukee pollution levels exceeded those that could reasonably be explained by local sources.

5.1. Calculation of Air Pollution Trajectories

An air pollution trajectory is the path followed by the average particle released from a particular point at a particular time and constrained to move with the wind. Only the specifically calculated winds are employed, the effects of turbulence are neglected. In the field, balloon tracking gives information on pollutant trajectories, although because of their inertia and buoyancy properties they are not normally able to follow air motions, and particularly vertical motions, with complete veracity.

Computer models produce values of wind at discrete points and times. Calculation of trajectories relies on interpolating winds so produced and moving a particle to follow the wind at that point. In general, a four-dimensional interpolation is required. Particle displacements are calculated for short timesteps. These are chosen to be sufficiently short that decreasing them any further does not influence significantly the course of the trajectory.

In the calculations which follow the interpolation was performed using a spline-under-tension. Because of the spatial symmetry of the particular problem investigated here a simple two-dimensional (one spatial and one temporal) routine was employed, the NCAR Scientific Subroutine Package "SURF". Accessability of NCAR Subroutines on the AES CYBER System has been documented by Reid and Boisvert (1976).

5.2. North Coast Case Study

The flow solution for the heated north coast situation discussed in the previous chapter is employed to drive the trajectory model. Since the situation lacks any variation in the x (along geostrophic wind) direction only one column normal to the coastline is considered at any one time. Further, since we are primarily interested in low level trajectories, which is where pollution is emitted, vertical motions are neglected. Figure 4.3 shows that vertical velocities are quite weak over land for this situation prior to about 11:30 a.m. and over the lake for most of the period. Thus we can expect that results for trajectories will be misleading over land after 11:30 a.m. The trajectories calculated are shown in Fig. 5.1. Trajectory origins 1/2 km inland from the coast at 8:00 a.m., 8:30 a.m., 9:00 a.m. and 10:00 a.m. are considered.

Trajectories starting at times up to 8:00 a.m. proceed slowly off-shore, failing to be markedly influenced by the lake-breeze circulation by the end of the time period. Only the initial portion of the trajectory is shown. The trajectory starting at 8:30 a.m. proceeds off-shore under the prevailing flow, but is overtaken by the lake-breeze effect and turns back toward land at 1:45 p.m. making a landfall just before 3:00 p.m. This is a long over-water trajectory so that deposition mechanisms would have a chance to deplete pollutant, but it should be noticed that the trajectory is under subsiding motion for most of its length suggesting that vertical dispersion would be suppressed.

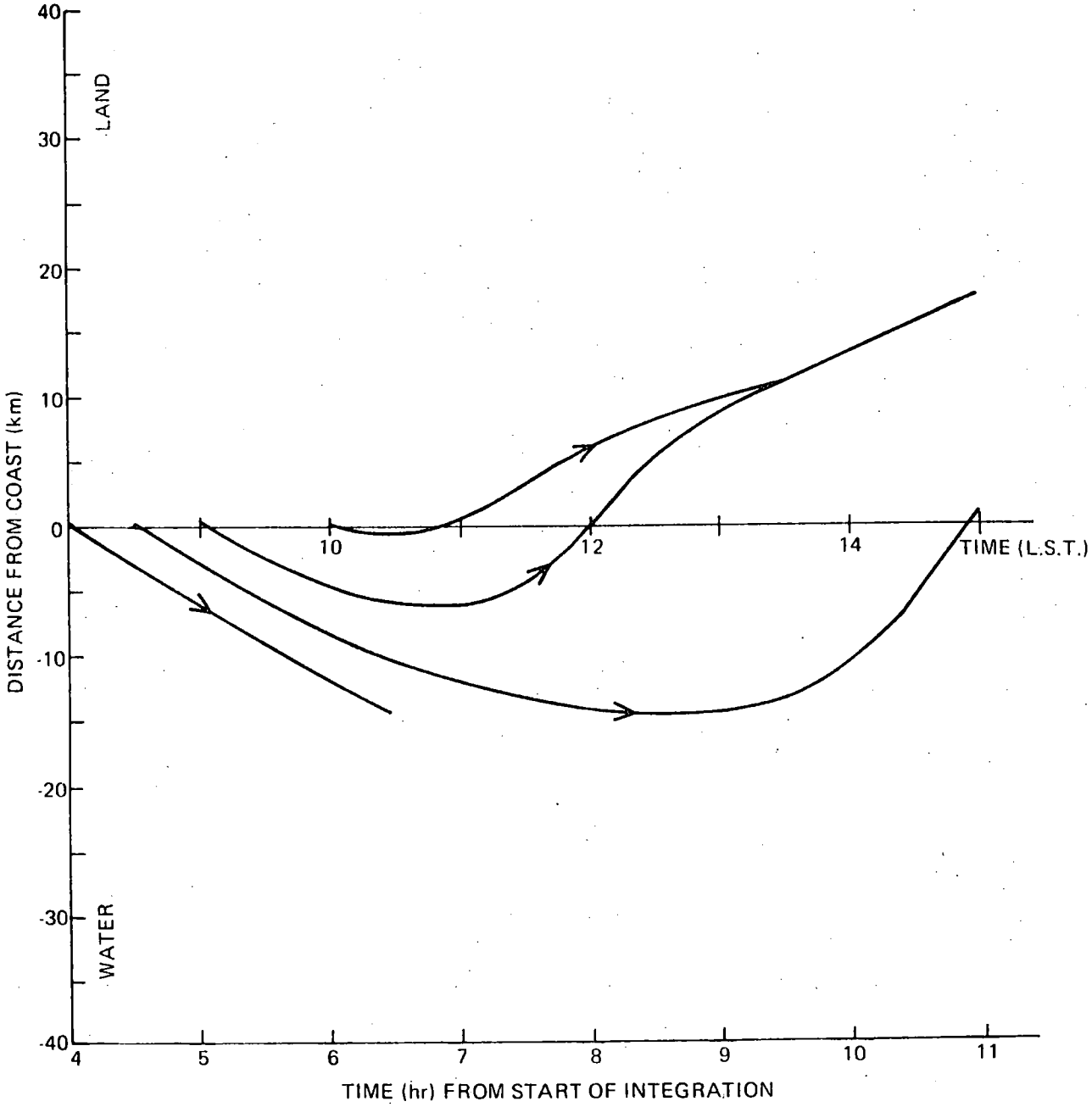

Figure 5.1. Pollution Trajectories for the Lake Breeze Experiment.

Only one-half hour later a trajectory started from the same location moves out over the lake only about 6 km before doubling back toward land, crossing the coast near noon. It is interesting that the 8:30 a.m. and 9:00 a.m. trajectories return to the coast three hours apart, but onshore wind speeds are still significant during this three hour period. Clearly this air is supplied by the (presumably relatively clean) subsiding air which has a maximum between these two trajectories.

The trajectory starting at 10:00 a.m. moves along the coast as the lake-breeze sets in for nearly one hour before moving inland. If the coastal strip is a high pollutant source region, as is often the case, this trajectory coupled with destabilization leading to fumigation will result in high ambient air pollution levels.

To summarize the pollution conditions inland of a coastal strip pollution source, the temporal variation seems fairly complex. Prior to the onset of the lake-breeze the pollutant emitted is advected out over the lake and inland pollution levels are at background. As the lake-breeze sets in high ambient air pollution levels are to be expected due to along-coast air trajectories. Up until one and half-hours after, this ambient pollution level should gradually decrease as each air parcel effectively gets a double dose of pollutant, but the first dose moves progressively further "upwind". The hours between noon and 3:00 p.m. should see improved air quality as subsident air from aloft over the water feeds inland. However, it may be that some of this has been cycled through lake-breeze direct circulation and thus contains pollutant. After 3:00 p.m., largely "double dose pollutant" air will again be crossing the coast, but its overwater trajectory is rather long so that air quality would only likely be moderately elevated above that for completely clean air crossing the coast.

5.3. Potential for Extended Application

The preceeding example has illustrated the potential for mesoscale modelling in air quality studies. Quite apart from the airflow model deficiencies noted previously this study has deficiencies. Firstly, three-dimensional trajectories (one horizontal, one vertical and one temporal dimension) would provide further insight, particularly with respect to the impact on air quality of subsiding air over the ocean. Secondly, only one prevailing geostrophic wind has been investigated. When a more reliable airflow model is developed, studies should be made for a variety of wind directions and speeds. In this regard, the coordinated modelling and observational studies of the lake breeze of the Lake Ontario shore of New York State by Estoque et al. (1976) are of direct relevance. The situation investigated involved an off-shore geostrophic wind component. Although trajectory studies were not made, indications from the winds given in their paper are that the sea-breeze for this case is not as effective as far off-shore as in the simulation presented here.

Insightful as trajectory studies such as these may prove, the real potential of such modelling must rest on inclusion of sub-grid scale motions integrated with explicitly modelled motions to predict turbulent dispersion. The direct extensions of the trajectory studies illustrated here to the prediction of air quality are the Particle-in-Cell (PIC) Method developed by Sklarew et al. (1971) and a very similar technique, the Monte Carlo Method developed by Thompson (1971), Reid (1974, 1976) and Watson and Barr (1976).

CHAPTER VI

6. SUMMARY AND CONCLUSIONS

The overall objective of this report has been to document advances during 1976 in three-dimensional and time-dependent mesoscale numerical modelling within the Boundary Layer Research Division. In particular, this effort is undertaken in support of the Air Quality and Inter-Environmental Research Branch's continuing effort to improve ability to assess air quality. In the following section this research is summarized especially as it impacts on Branch objectives. General conclusions regarding mesoscale modelling and specific conclusions regarding the Pielke model are noted. Finally, plans for continuation of these studies are outlined.

6.1. Summary

Although currently employed air quality models are sound, their range of validity is limited. More broadly-based methods for air quality assessment are required. Numerical modelling of mesoscale pollutant transport process, the most pressing need for understanding ambient air quality, is still in its infancy and not yet ready for application. However, prospects are bright that a useful modelling capability applicable to actual topographic situations can be developed. Meanwhile important insights can be gained through simulation studies.

The Pielke model, developed in some detail herein, has grave limitations for air quality purposes but can still provide improved understanding for a limited range of conditions. This capability is demonstrated in the coastal pollution trajectory study which is to be expanded in the near future.

Development of an improved model will require additional manpower commitments. Timely solution of the scientific problems which inevitably will be encountered (a specific example is incorporation of an efficient surface energy budget) will require an additional research scientist devoted to this effort. The complexities of the computer programming demand that a skilled programmer, with a good knowledge of the CYBER 76, be assigned.

6.2. General Conclusions

(a) Three-dimensional and time-dependent mesoscale modelling is feasible on the AES CYBER computer system, although it strains the machine capacity.

(b) Simulation experiments with such a model provide a rapid means to gather valuable qualitative understanding of specific classes of pollutant transport situations.

(c) Simplifying assumptions, such as eddy viscosity closure and the hydrostatic assumption, are appropriate on this scale, particularly for gentle topography and neutral or stable stratification conditions.

(d) The surface energy budget is often intimately involved with airflow evolution and needs to be given careful explicit attention.

(e) For cases with significant surface forcing the qualitative nature of airflow evolution is not greatly influenced by the nature of the initial boundary layer wind profile.

(f) A detailed diagnostic treatment of model kinetic and potential energy budgets is essential in establishing veracity of model simulations.

6.3. Specific Conclusions Regarding the Pielke Model

The Pielke model suffers from a number of serious deficiencies including:

(a) Numerical upstream differencing.

(b) Inadequate treatment of boundary conditions.

(c) Lack of an explicit surface energy budget.

(d) Lack of moisture processes.

(e) Lack of a diagnostic assessment of model energy budgets.

(f) Inadequate treatment of the boundary layer to account for limited vertical resolution.

6.4. Plans

Preliminary investigations have been instituted to study alternative numerical techniques. Finite element and spectral methods are under consideration along with more sophisticated finite difference schemes. These will undoubtedly involve additional computer overhead beyond that used with upstream differencing. A careful evaluation of advantages and disadvantages will be required in selecting an optimum scheme. Factors to be considered will include computer execution time, required core storage, and accuracy of computation.

The strong evidence from this study of the importance of boundary conditions demands this factor be particularly carefully studied. The selection of boundary conditions is closely tied in with the selection of numerical integration technique. Inflow boundaries appear to be the most troublesome. Alternative approaches need to be evaluated. Some success has been reported using a stretching of the horizontal grid toward the boundaries.

Initial investigations of energy budget calculations have been made. Indications are that this will add significantly to computer storage and computational requirements. Optimization of these aspects will constitute one of the greatest challenges of this program.

It is clear that the results of this study are encouraging for further development of mesoscale modelling for air quality purposes. It is equally clear that the Pielke model has too many inadequacies for reliable use. To meet these objections development of a new model, based on the experience gained with the Pielke model, is planned.

References

Busch, N.E., 1973: On the Mechanics of Atmospheric Turbulence in Workshop on Micrometeorology, D.A. Haugen (ed.), Am. Meteor. Soc., Boston, pp. 1-65.

Clarke, R.H., 1970: Recommended methods for the treatment of the boundary layer in numerical models. Australian Meteor. Mag., 18, 51-73.

Deardorff, J.W., 1973: Three-Dimensional Numerical Modeling of the Planetary Boundary Layer, in Workshop on Micrometeorology, D.A. Haugen (ed.), Am. Meteor. Soc., Boston, pp. 271-311.

_____, 1974: Three-dimensional numerical study of the height and mean structure of a heated planetary boundary layer. Bound.-Layer Meteor., 7, 81-106.

Estoque, M.A., J. Gross and H.W. Lai, 1976: A Lake Breeze over Southern Lake Ontario. Mon. Wea. Rev., 104, 386-396.

Haltiner, G.J., 1971: Numerical Weather Predictions. Wiley, New York, 317 pp.

Hino, M., 1968: Computer Experiment on Smoke Diffusion Over a Complicated Topography. Atmos. Environment, 2, 541-558.

Keyser, D. and R. Anthes, 1976: Sensitivity Tests with a Parameterized Mixed-Layer Model Suitable for Air Quality Simulations, presented at EPA Conference on Environmental Modeling and Simulation, Cincinnati, Ohio, April 19-22, 1976.

Klemp, J.B. and D.K. Lilly, 1975: The Dynamics of Wave-Induced Downslope Winds. J. Atmos. Sci., 32, 320-339.

Kwizak, M. and A.J. Robert, 1971: A Semi-Implicit Scheme for Grid Point Atmospheric Models of the Primitive Equations. Mon. Wea. Rev., 99, 32-36.

Lavoie, R.L., 1972: A Mesoscale Numerical Model of Lake-Effect Storms. J. Atmos. Sci., 29, 1025-1040.

Liu, M. and J. Seinfeld, 1974: A Comparison of the Grid and Trajectory Models of Urban Air Pollution, Proceedings, Symposium on Atmospheric Diffusion and Air Pollution, Santa Barbara, September 9-13, 1974, pp. 303-310.

Lumley, J.L. and B. Khajeh-Nouri, 1974: Computational Modeling of Turbulent Transport. Adv. Geophys., 18A, 169-192.

Lyons, W.A. and H.S. Cole, 1976: Photochemical Oxidant Transport: Mesoscale Lake Breeze and Synoptic-Scale Aspects, J. Appl. Meteor., 15, 733-743.

Mahrer, Y. and R. Pielke, 1975: A Numerical Study of the Air Flow Over Mountains Using the Two-Dimensional Version of the University of Virginia Mesoscale Model. J. Atmos. Sci., 32, 2144-2155.

_____ and _____, 1976: Numerical Simulation of the Airflow Over Barbados. Submitted for publication.

McBean, G.A., 1976: The Influences of Surface Roughness, Vertical Thermal Stability and Wind on the Boundary Layer Fluxes of Momentum, Heat and Water Vapour: A Review, in Final Report W.M.O. Commission for Atmospheric Sciences Working Group on Atmospheric Boundary Layer Problems. In press.

Monin, A.S. and A.M. Yaglom, 1971: Statistical Fluid Mechanics: Mechanics of Turbulence, 1. MIT Press, Cambridge Mass., 769 pp. (Originally published in Russian in 1965 by Nauka Press, Moscow).

O'Brien, J.J., 1970: A Note on the Vertical Structure of the Eddy Exchange Coefficient in the Planetary Boundary Layer. J. Atmos. Sci., 27, 1213-1215.

Phillips, N.A., 1957: A Co-ordinate System having some Special Advantages for Numerical Forecasting. J. Meteor., 14, 184-185.

Pielke, R.A., 1972: Comparison of a Hydrostatic and an Anelastic Dry Shallow Primitive Equation Model. NOAA Tech. Mem. ERL-OD-13, 47 pp.

_____, 1973: A three dimensional numerical model of the sea breezes over South Florida. Ph.D. dissertation, The Pennsylvannia State University, 135 pp.

_____, 1974a: A Three-Dimensional Numerical Model of the Sea Breeze over South Florida. Mon. Wea. Rev., 102, 115-139.

_____, 1974b: A Comparison of Three-Dimensional and Two-Dimensional Numerical Predictions of Sea Breezes. J. Atmos. Sci., 31, 1577-1585.

Pielke, R.A. and Y. Mahrer, 1975: Representation of the Heated Planetary Boundary Layer in Mesoscale Models with Coarse Vertical Resolution. J. Atmos. Sci., 32, 2288-2308.

Reid, J.D., 1974: Predicting Nucleant Concentrations from Ground Based Generators. Proceedings, Fourth Conference on Weather Modification. November 18-21, 1974, Fort Lauderdale, Fla., pp. 447-453.

_____, 1976: Dispersion in a Mountain Environment. Ph.D. Dissertation, Dept. of Atmospheric Science, Colorado State University.

_____ and G. Boisvert, 1976: NCAR Scientific Subroutines available on AES CYBER. Contact, December 1976, Can. Meteor. Centre, Atmos. Environment Service, Montreal.

Richtmyer, R.D. and K.W. Morton, 1967: Difference Methods for Initial-Value Problems, (2nd ed.) Interscience Pub., New York.

Shershkov, V.V., 1972: One Method of Computing the Meteorological Variables for Mesoscale Processes. Izv. Atmos. Ocean. Phys., 8, 695-703.

Sklarew, R.C., A.J. Fabrick and J.E. Prager, 1971: A Particle in Cell Method for Numerical Solution of the Atmospheric Diffusion Equation, and Applications to Air Pollution Problems. Systems, Science and Software Rept. 3SR-844-I, EPA Contract 68-02-0006.

Smagorinsky, J., 1963: General Circulation Experiments with the Primitive Equations: Part I, The Basic Experiment. Mon. Wea. Rev., 91, 99-164.

Summers, P.W., 1964: An Urban Ventilation Model Application to Montreal. Ph.D. Dissertation, McGill University, 159 pp.

Taylor, P.A., 1976: Numerical Studies of Neutrally Stratified Planetary Boundary-Layer Flow Above Gentle Topography. Part I: Two-Dimensional Cases. Submitted to Boundary-Layer Meteor.

_____ and Y. Delage, 1971: A Note on Finite-Difference Schemes for the Surface and Planetary Boundary Layers. Boundary-Layer Meteor., 2, 108-121.

Thompson, R., 1971: Numeric Calculation of Turbulent Diffusion. Quart. J. Roy. Meteor. Soc., 97, 93-98.

Thyer, N.H., 1967: A Theoretical Explanation of Mountain and Valley Winds by a Numerical Method. Arch. Met. Geoph. Biokl., Ser. A., 14, 318-348.

Walmsley, J.L., 1976: A Second-Order-Closure Model of Wind and Turbulence for Use in the Atmospheric Environment Service. Internal Report ARQT-1-76. AES, Downsview, Ontario.

Watson, C.W. and S. Barr, 1976: Monte Carlo Simulation of the Turbulent Transport of Airborne Contaminants. Los Alamos Sci. Lab. Rept. LA-6103, January 1976, 28 pp.

Wyngaard, J.C. and O.R. Coté, 1974: The Evolution of a Convective Planetary Boundary Layer - a Higher-Order-Closure Model Study. Boundary-Layer Meteor., 7, 289-308.

Yamada, T. and G. Mellor, 1975: A Simulation of the Wangara Atmospheric Boundary Layer Data. J. Atmos. Sci., 32, 2309-2329.

Yamamoto, G. and A. Shimamuki, 1966: Turbulent transfer in diabatic conditions. J. Meteor. Soc. Japan, 44, 301-307.